Fitting and Using Model Hamiltonian in non-adiabatic Molecular Dynamics Simulations

by

Jonathan Ross Smale

A thesis submitted to
the University of Birmingham
for the examination of
DOCTOR OF PHILOSOPHY

School of Chemistry
University of Birmingham
2011

Abstract

In order to study computationally increasingly complex systems using theoretical methods model Hamiltonians are required to accurately describe the potential energy surface they represent. Also ab-initio methods improve the calculation of the excited states of these complex systems becomes increasingly feasible. One such model Hamiltonian described herein, the Vibronic Coupling Hamiltonian, has previously shown its versitility and ability to describe a variety of non-adiabatic problems. This thesis describes a new method, a genetic algorithm, for the parameterisation of the Vibronic Coupling Hamiltonian to describe both previously calculated potential energy surfaces (allene and pentatetraene) and newly calculated (cyclo-butadiene and toluene) potential energy surfaces. In order to test this genetic algorithm quantum nuclear dynamics calculations were performed using the multi-configurational time dependent hartree method and the results compared to experiment.

For my family, whose love and support was indispensible throughout the course of this thesis.

Acknowledgements

I would like to thank all of the following people for their contribution to my education and my life over the last four years.

My supervisor Graham, without whose patience, wisdom and optimism this thesis would not have been possible

My fellow chemists, those in the Worth group, the physical chemists of the second floor and the countless others who have put up with me other the years. In particular I would like to thank those who helped me so much in the beginning, Tom and Kousik for numerous insights into what exactly it was I was studying.

This thesis and the work described in it are entirely my own, except where I have acknowledged *either* help from a named person *or* a reference is given to a published source or a thesis. Text taken from another source will be enclosed in quotation marks and a reference will be given.

October 1, 2012

Contents

List of Figures

List of Tables

Glossary

ADC Algebraic Diagrammatic Construction

CASPT2 Complete Active Space with 2^{nd} Order Perturbation

CASSCF Complete Active Space Self Consistant Field

DOF Degrees of Freedom

DVR Discrete Variational Representation

FBR Finite Basis Representation

HF Hartree-Fock

HF-SCF Hartree-Fock Self Consistant Field

MP2 Second order Moller-Plesset pertubation theory

MP4 Forth order Moller-Plesset pertubation theory

OVG Outer Valence Greens Function

PES Potential Energy Surface

SPF Single Particle Function

TDH Time Dependent Hartree

TDSE Time Dependent Schrödinger

TISE Time Independent Schrödinger

Chapter 1

Introduction

The study of photochemistry can be applied to a wide variety of everyday life. From photosynthesis, which accounts for the production of all of our food and air [1], to the balance of greenhouse gases in our atmosphere [2]. In its simplest terms photochemistry is the interaction of light with a molecule leading to the generation of a molecule in an excited state [3]. These excited states have properties, their energies and lifetimes, which are entirely dependent of the electronic and nuclear configuration on that state. We can therefore consider all of photochemistry as the study of the time evolution of the nuclear and electronic structure following excitation by a radiation field [4].

A variety of photochemical processes can occur following this initial excitation, a summary of these is depicted in figure 1.1. The intial excitation can also be termed absorbance, as it can also be described as the absorbance of a photon. This is a very fast transition of the time scale of $\sim 10^{-15}$ s. This is a type of radiative process, two other radiative processes can then occur namely fluorescence and phosphorescence. Flourescence is the emission of a photon from an electronically excited singlet electronic state and occurs

on the time scale $\sim 10^{-8}$ s. Phosphorescence is the emission of a photon from an electronically excited triplet state, which is a spin forbidden process and as such occurs on a much slower time scale of $\sim 10^{-3}$ s. Spin forbidden processes are discussed further in the Symmetry and Group Theory Section 2.5.

The energy can also be redistributed within the molecule by a number of non-radiative processes. Two of these are depicted in figure 1.1. Internal conversion is the non-radiative process where the energy, or wavepacket, moves to a lower energy excited state and is of the time scale $\sim 10^{-12}$ s. This occurs when a vibrational state of an excited state can couple with a vibrational state of a lower energy excited state. Internal Conversion (IC) is a spin allowed transition, when the wavepacket moves from an excited state to a lower energy excited state of a different spin multiplicity this is termed Intersystem Crossing (ISC). As this transition is spin forbidden it occurs on a much slower time scale of $\sim 10^{-3}$ s to $\sim 10^{-1}$ s. Unlike Internal Conversion, where coupling between vibrations allows the transition, Intersystem Crossing occurs as a result of spin-orbit coupling (In small atoms this is between the total spin angular momentum and the total orbital angular momentum.)

Other non radiative processes can occur, most typically vibrational relaxation where the energy is transferred to its surroundings (which cannot occur for isolated molecules), Intramolecular Vibrational Relaxation (IVR) where a localised vibrational excitation is irreversibly dissipated (relaxed) throughout the molecule and by passing through a Conical Intersection (CI), which in a two dimensional system, is an intersection between two potential energy surfaces (when their energies become degenerate) which allows the energy to return to a lower energy electronic state without emitting a photon (unlike flourescence and phosphorescence which also return the molecule to a lower

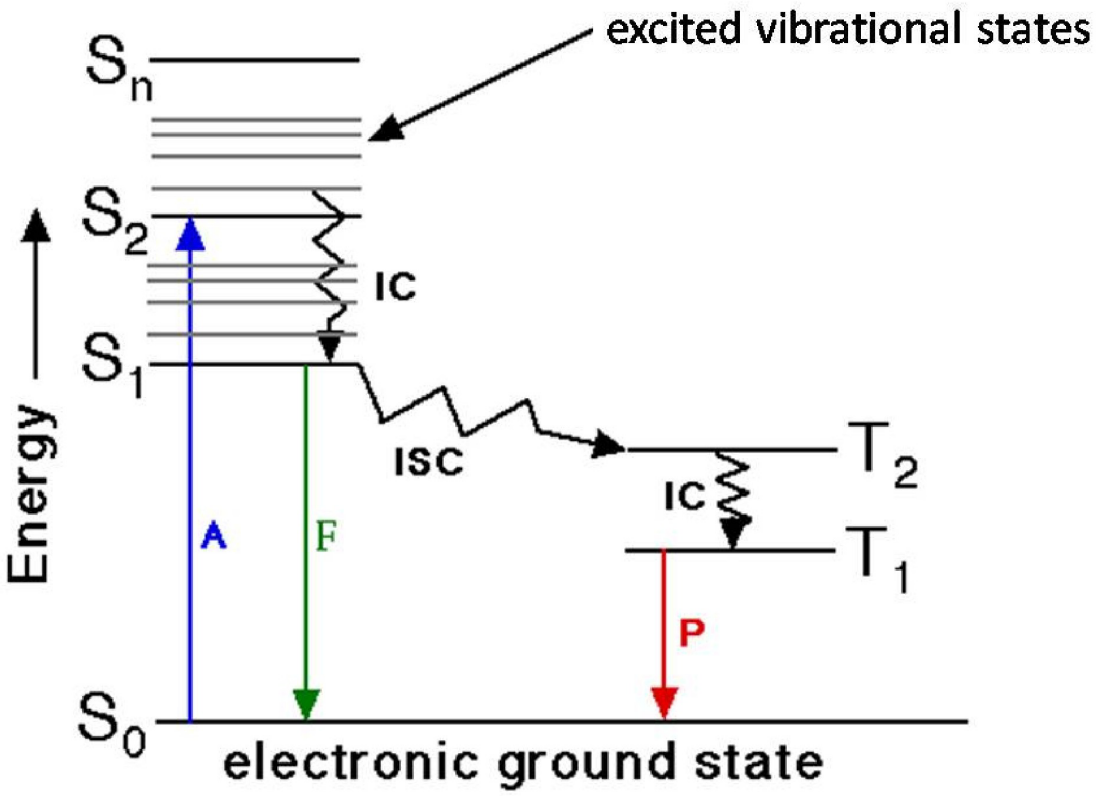

Fig. 1.1: A diagram depiciting the electronic states of a molecule and the photochemical processes between them, where S_i is the singlet state i, T_i is the triplet state i, A is Absorbance, F is fluorescence, P is phosphorescence, IC is Internal conversion and ISC is Intersystem Crossing.

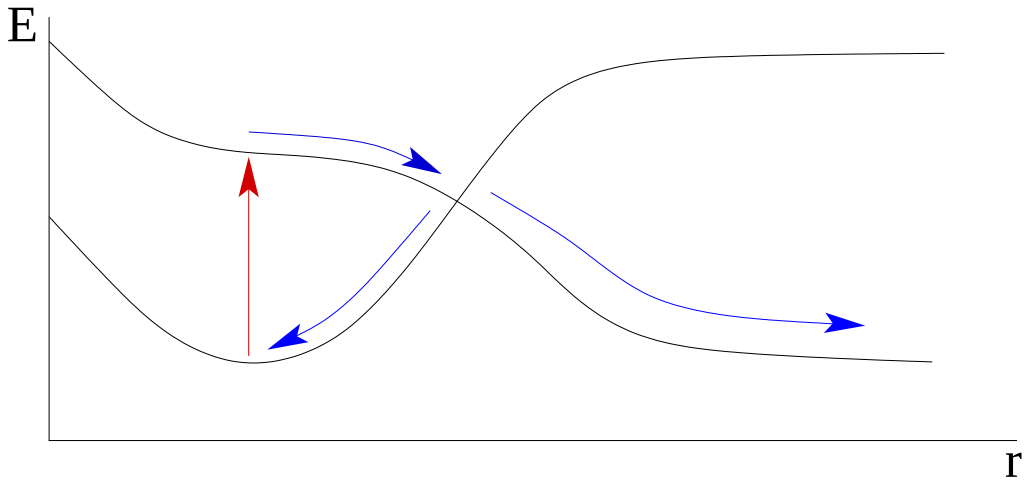

Fig. 1.2: A diagram depiciting a simple conical intersection where E is the energy and r is a reaction co-ordinate. The red arrow depicts absorbance of a photon to an excited state and the blue arrow depicts the path the wavepacket can take through the conical intersection to return to the ground state.

electronic state). This is demonstrated in figure 1.2 and discussed further in section 2.6.

These processes can be examined experimentally by measuring the radiation intensity as a function of the wavelength, this is termed spectroscopy. As the resonant frequencies have large amplitudes they can be identified using spectroscopic methods. In Quantum Mechanical terms one can say that the coupling between an atom/molecule and a photon is analogous to a resonance. As the coupling between an atom/molecule is strongest when the energy of the photon matches the energy difference between two states, the spectrum can be used to experimentally determine the energy difference between states. In order to determine the rates of these processes it is neccessary to perform time-resolved spectroscopy.

Time-resolved spectroscopy has advanced leaps and bounds with numerous technological developments. From simple shuttered appertures to flash bulbs and finally laser pulses the study of chemistry has advanced rapidly,

and with every advance we are able to look in a greater time resolution than before. Recent improvments in experimental techniques, particularly the pump-probe scheme developed by Zewail [5, 6], has allowed chemists to explore the time-evolution of a wavepacket on the femto second time regime. In the pump-probe scheme developed by Zewail [5, 6] an electronically excited state that one wishes to examine is prepared with a laser pule, the pump pulse, and then probed with a second laser pulse at a fixed time delay. By performing this experiment with a variety of time delays one achieves a time resolved spectrum.

The first example ultrafast spectroscopy, that is time resolved spectroscopy on the fempto second time scale, was the study of the bond breaking dynamics of I-CN [7]. A schematic representation of the potential energy surface is shown in figure 1.3 and the spectroscopic results are shown in figure 1.4. This method has been used for a variety of systems [6] using a number of spectroscopic techniques.

The spectra shown in figure 1.4 are produced using laser induced floures-cence, where a molecule is excited by a laser and after a short period of time (typically on the order of nanoseconds) the excited species (in this case an ion) emits a photon which is then deteced. As the laser induced flourescence is related to the Frank Condon (FC) overlap one can determine the motion of the wavepacket from the ion yeild. Another important technique used in ultrafast spectroscopy is time resolved photoelectron spectroscopy, where the second laser pulse (probe pulse) ionises the target molecule and the kinetic energy of the resulting electron is measured. One can use this kinetic energy to determine the binding energy (the energy required to remove an electron from its atomic/molecular orbital) using the relationship expressed

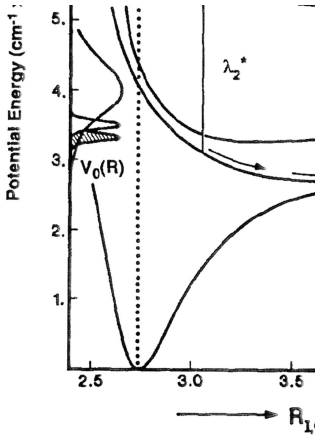

Fig. 1.3: A simplification of the potential energy surface of I-CN, the pump pulse causes a vertical transition from V_0 to V_1 and the motion of the wavepacket after is indicated by the arrows. Reproduced from [7].

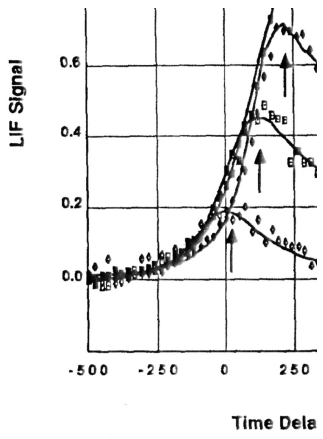

Fig. 1.4: Experimental results showing the spectra for 4 different time delays superimposed on each other. The spectra show the I-CN bond stretching and breaking after excitation. Reproduced from [6].

in equation 1.1.

$$E_k = h\upsilon - E_b \tag{1.1}$$

where E_k is the kinetic energy of the ejected electron, h is Planck's constant, υ is the wavelength of the photon causing the ejection of the electron and E_b is the binding energy.

The data produced from spectroscopic techniques is extensive and it is here that theoretical methods can help to explain the observed results. In order to do this we need to solve the time dependent Schrödinger equation so that we may propagate a wavepacket across a potential energy surface. These wavepacket dynamics calculations are only possible for molecules with a single electron, unless approximations are used. One such approximation is the Multi-Configurational Time Dependent Hartree method (MCTDH) [8].

In order to use these methods we must first have a potential energy surface to propagate our wavepacket on. The calculation of electronically excited states is a difficult problem in the field of theoretical chemistry [9]. Although many computational methods exist in order to calculate these excited state energies, they are computationally expensive and fraught with other problems (which are discussed in later chapters). Once we have these potential energy surfaces we need them in a form which can be quickly analysed by our wave propogation method, usually in the form of a mathematical function.

One such example is the Vibronic Coupling Hamiltonian (VCHAM) which has been frequently used [10–12] to describe a number of non-adiabatic problems such as Intramolecular Vibrational Relaxation which is discussed in chapter 6. The VCHAM is well suited as a general purpose Hamiltonian

due to its simple formulation. So far the VCHAM has been used for a wide variety of simple examples of non-adiabatic problems. For larger problems the VCHAM becomes more difficult to use as it increasingly has a vast number of parameters. In order to use the VCHAM these parameters must be optimized to fit the calculated excited state energies.

The optimisation of these parameters forms a major part of this thesis. Ideally we would like to have the perfect set of parameters to minimise the difference between the model Hamiltonian and the calculated excited state energies; this 'perfect set' is the global minimum. Unfortunately simple optimisation routines are only able to find a local minimum, that being the nearest minimum to their initial starting value. The development of a global optimisation technique, specifically a genetic algorithm, its applications and a variety of test cases are presented here.

In the course of this thesis several molecules are discussed, of particular important are the molecules cyclobutadiene, allene, pentatetraene and toluene (their structures are shown in figure 1.5). With the exception of toluene these molecules are used as test cases for the genetic algorithm developed as part of my doctoral studies. Cyclobutadiene has been studied extensively experimentally [13–15] and theoretically [12, 16–18] due to interesting nature of it's ground state. As it is a ring with 4 π electrons Hückel's rule would predict that cyclobutadiene would be unstable, anti aromatic and have a triplet ground state. However both experimental [13] and theoretical studies [18] have shown that there is a nonplanar rectangular distotion to a singlet ground state. This is caused by the Jahn-Teller effect which is discussed in section 2.6. Allene and Pentatetraene were both originally in-

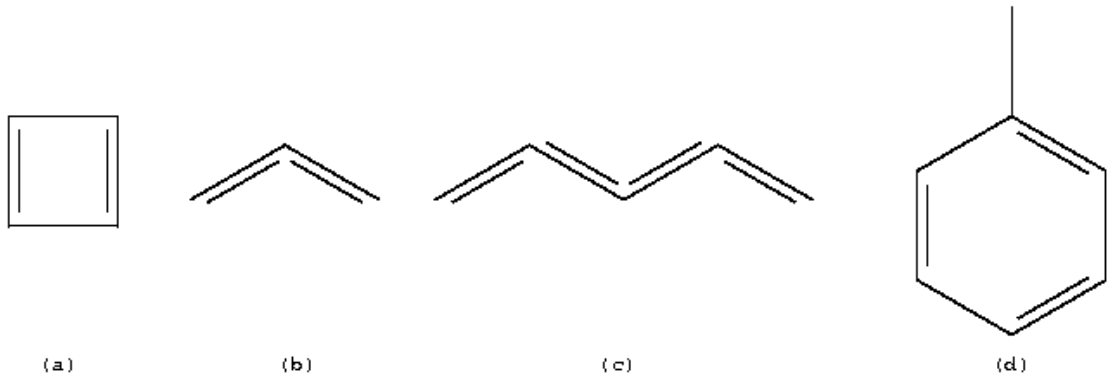

Fig. 1.5: A diagram showing the chemical structures of the molecules discussed in detail in this thesis, where (a) is cyclobutadiene, (b) is allene, (c) is pentatetraene and (d) is toluene.

vestigated due to the presence of Jahn-Teller coupling 2.6 and their interest as molecular wires [10, 11]

Chapter 2

Background Theory

In this chapter the theory underlying the research reported and the computational methods described in the subsequent chapters is disscussed. The main theory presented is the Schödinger equation and its two main forms, the time dependent and time independent perspective. The time independent Schrödinger equation is used for electronic structure methods which describe the energetics of the system of interest. In the subsequent chapters these energetics are calculated at a variety of geometries in order to build up a potential energy surface (PES). The time dependent Schrödinger equation is used for the dynamic calculations, where a wavepacket is propagated accross the potential energy surface.

It is not feasible to solve the Schrödinger equation exactly for systems containing more than a few electrons due to the size of wavefunction needed to describe it. The complexity of the decription increases dramatically with the number of degrees of freedom (DOF) and the size of the basis set and requires the use of approximations. Once such approximation commonly used and discussed below is the Born-Oppenheimer approximation.

2.1 Schrödinger Equation

The Schrödinger equation was devised by Erwin Schödinger in 1926 [19] as a way of describing how the quantum state of a physical system changes in time. This quantum state, usually referred to as the wavefunction (Ψ) is a complete description of the physical system. In its time dependent form the Schrödinger equation describes the time evolution of the system and where the Hamiltonian is not explicitly dependent of time (in a stationary state) the time independent form can also be used. The time dependent Schrödinger equation (TDSE) can be written

$$-i\hbar\frac{\partial\Psi(r,t)}{\partial t} = \hat{H}\Psi(r,t) \tag{2.1}$$

and the Hamiltonian operator ($\hat{H}$) is written:

$$\hat{H} = -\frac{\hbar^2}{2\mu_i}\nabla_i^2 + V(r) \tag{2.2}$$

i is $\sqrt{-1}$ and $\hbar$ is Plancks constant divided by 2π.

$$\Psi(r,t) = \psi(r)T(t) \tag{2.3}$$

where ψ(r) is the spatial wavefunction and T(t) is the temporal part. Substituting equation 2.3 into equation 2.1 and dividing by the overall wavefunction we obtain two equations:

$$-i\hbar\frac{\partial T(t)}{\partial t} = ET(t) \tag{2.4a}$$

$$\hat{H}\psi(r) = E\psi(r) \tag{2.4b}$$

Equation 2.4b is the time independent Schrödinger equation. This equation is an example of an eigenvalue equation. E is the eigenvalue and can take on certain discrete values depending on the eigenfunction ψ and linear operator $\hat{H}$. Equation 2.4a can be developed to give the solution:

$$T(t) = T_0 \exp^{-iEt/\hbar} \tag{2.5}$$

We may now write the solutions of the TDSE as

$$\Psi(x,t) = \psi(r) T_0 \exp^{-iEt/\hbar} \tag{2.6}$$

This describes the time evolution of the wavefunction. T_0 is the initial temporal wavefunction which can be absorbed into $\psi(r)$.

2.2 Born-Oppenheimer Approximation

The Born-Oppenheimer Approximation was proposed by Max Born and J. Robert Oppenheimer in 1927 [20] as a way of alleviating the huge effort required to solve the Schödinger equation for molecules larger than H_2. This is achieved by separating the electronic parts of the wavefunction from the nuclear parts. In its simplest form can be expressed as:

$$\Psi_{total} = \Psi_{nuclear} \Psi_{electronic} \tag{2.7}$$

Physically this represents the electrons moving in the static field of the nuclei and ignores any correlation between the two. As electrons move significantly faster than nuclei, relatively, this approximation is reasonable but many quantum effects occuring on or near this time scale require some de-

scription of this correlation as will be shown later. One can describe the Hamiltonian in this approximation in terms of the kinetic and potential energy terms:

$$H = T_e + T_N + V_e + V_N + V_{eN} \tag{2.8a}$$

$$H = \sum_i -\frac{\hbar^2}{2m}\frac{\partial^2}{\partial r_i^2} + \sum_i -\frac{\hbar^2}{2M_i}\frac{\partial^2}{\partial R_i^2} + \sum_{j>i}\frac{e^2}{|r_i - r_j|} + \sum_{j>i}\frac{Z_i Z_j e^2}{|R_i - R_j|} - \sum_{ij}\frac{Z_j e^2}{|r_i - R_j|} \tag{2.8b}$$

T_e and T_N are the kinetic energy terms for the electrons and nuclei, V_e and V_N are the potential energy terms for the electrons and nuclei and V_{eN} is the nuclear-electronic potential coupling term. R_i, $\frac{\partial^2}{\partial R_i^2}$ are the nuclear position and momentum, Z_i is the nuclear charge and r_i, $\frac{\partial^2}{\partial r_i^2}$ are the electronic position and momentum.

Equation 2.8b shows that even in the simplest molecule, it is very computationally expensive to solve the Schrödinger equation analytically due to the large number of terms. An approximation to overcome this difficulty to use the vast difference between the mass of the electrons and the nuclei [20]. The mass difference means that the position of the electrons will effectively change instantly with respect to any change in the nuclear geometry. This allows us to consider the nuclear geometry as fixed, and so solve the Schrödinger equation. This can be shown by expressing the full wavefunction as:

$$\Psi(r;R) = \psi(r;R)\chi(R) \tag{2.9}$$

Substituting equation 2.9 into equation 2.4b with the Hamiltonian in equation 2.8b we obtain:

$$[\hat{T}_N(R) + \hat{T}_e(r) + \hat{V}_{eN}(r,R) + \hat{V}_{NN}(R) + \hat{V}_{ee}(r)]\psi(r;R)\chi(R) = E\psi(r;R)\chi(R) \tag{2.10}$$

since $\hat{T}_e$ contains no $\mathbf{R}$ dependence, we can write:

$$\hat{T}_e\psi(r;R)\chi(R) = \chi\hat{T}_e\psi \tag{2.11}$$

The same cannot be assumed for the nuclear kinetic energy term because it is dependent on $\mathbf{R}$, hence it must be expressed, using the product rule, as 2.12:

$$\frac{\partial^2}{\partial R^2}\psi(r;R)\chi(R) = \psi\frac{\partial^2}{\partial R^2}\chi + 2\frac{\partial}{\partial R}\psi\frac{\partial}{\partial R}\chi + \chi\frac{\partial^2}{\partial R^2}\psi \tag{2.12}$$

This is more commonly written as:

$$H\psi\chi = T_e\psi\chi + V_e\psi\chi + +V_N\psi\chi + V_{eN}\psi\chi + W = E\psi\chi \tag{2.13}$$

$$W = -\sum_j \frac{\hbar^2}{2m}(\psi\frac{\partial^2}{\partial R^2}\chi + 2\frac{\partial}{\partial R}\psi(r;R)\frac{\partial}{\partial R}\chi(R) + \chi\frac{\partial^2}{\partial R^2}\psi) \tag{2.14}$$

In equation 2.14 the last two terms involve derivatives of the electronic wave-function, with respect to nuclear coordinates, however both of these terms are proportional to the mass ratio between electrons and nuclei, and hence due to the massive difference in size these terms can be ignored. This means the Schrödinger equation in the Born-Oppenheimer approximation is written as:

$$\psi T_N\chi + (T_e\psi + V_e\psi + +V_N\psi + V_{eN}\psi)\chi = E\psi\chi \tag{2.15}$$

we may multiply on the left by ψ^* to yield the nuclear Schrödinger equation:

$$(T_N + V)\chi = E\chi \tag{2.16}$$

From equation 2.14 it is possible to deduce the limit of this approximation. It can be shown [21] and is described below in section 2.3.2 that the approximation breaks down when electronic states are close in energy. In excited states fast nuclear vibrations mean that the two neglected terms can no longer be ignored. This results in the coupling between nuclear and electronic motion and some interesting and important dynamical features.

2.3 The Adiabatic and Diabatic Picture

The section will introduce the basis of both the diabatic and adiabatic theories, as well as their definition. The Adiabatic theory [21, 22], for a quantum mechanical system, states that under slowly changing external conditions the system can adapt its functional form, where rapid changes leave no time for the system to adapt leaving the probabilty matrix unchanged. The diabatic theory however states that rapidly changing conditions do not allow time for the system to adapt, resulting in no change in the probability density. This results in there, typically, being no final eigenstate of the Hamiltonian with the same functional form as the initial state.

2.3.1 Adiabatic Representation

The adiabatic representation and limit can be shown by expressing the TDSE in the previously written form 2.1 where the Hamiltonian and wavefunction

are written as

$$H(t) = \begin{pmatrix} E_a & V_{ab}(t) & ... \\ V_{ba}(t) & E_b & ... \\ ... & ... & ... \end{pmatrix} \tag{2.17}$$

$$\Psi(t) = \begin{pmatrix} \Psi_a \\ \Psi_b \\ ... \end{pmatrix} \tag{2.18}$$

If V_{ab} and V_{ba} are small and therefore slowly changing, as we are assuming in the adiabatic representation, it is possible to write:

$$U^{-1}(t)H(t)U(t) = D(t) \tag{2.19}$$

$$U^{-1}\Psi = \Psi' \tag{2.20}$$

where U is a unitary evolution operator defined $\exp^{-iHt/\hbar}$, which transforms $\Psi(0)$ into $\Psi(t)$. The TDSE can be written:

$$i\hbar\frac{\partial}{\partial t}(U\Psi'(t)) = i\hbar\left(U(t)\frac{\partial\Psi'}{\partial t} + \frac{\partial U(t)}{\partial t}\Psi'\right) = H(t)U(t)\Psi'(t) \tag{2.21}$$

by multiplying through by U^{-1} it can be written in the form:

$$i\hbar\frac{\partial}{\partial t}(\Psi'(t)) = D(t)\Psi'(t) - i\hbar U^{-1}(t)\frac{\partial U(t)}{\partial t}\Psi' \tag{2.22}$$

and hence if H(t) is slow varying then so will U(t) and U^{-1}(t) meaning the second term on the right hand side will be small and can be neglected [21].

2.3.2 Non-adiabatic Corrections

The Born-Oppenheimer Approximation (BOA) in the presence of significant off-diagonal terms in the Hamiltonian matrix (representing strong coupling between two electronic states, typically close in enerrgy) means that it is no longer possible to ignore the right hand side term in equation 2.22. It is possible to simplify equation 2.22 so that the wavefunction is written:

$$\left(\hat{T}_N + V_i\right)|\Psi_i\rangle - \sum_j \Lambda_{ij}|\Psi_i\rangle = i\hbar\frac{\partial}{\partial t}|\Psi_i\rangle \tag{2.23}$$

where i and j represent the two states, and Λ_{ij} is the non-adiabatic coupling term which is written:

$$\Lambda_{ij} = \frac{\hbar^2}{2}(G_{ij} + 2F_{ij}\nabla) \tag{2.24}$$

where G_{ij} is a matrix which can be further broken down into the form

$$G_{ij} = \nabla + F_{ij} + \sum_k F_{ik}.F_{kj} \tag{2.25}$$

This shows that the force matrix F_{ij} is the defining quantity in the strength of the non-adiabatic coupling, which itself is dependent on the energy gap between the two states:

$$F_{ij} = \frac{1}{\sqrt{M}}\frac{1}{V_j - V_i}\langle\psi_i|\frac{\partial\tilde{H}_{el}}{\partial R}|\psi_j\rangle \tag{2.26}$$

where M is the mass, $V_j - V_i$ is the gap between the two states and $\langle\psi_i|\frac{\partial\tilde{H}_{el}}{\partial R}|\psi_j\rangle$ is the force between the two states as a function of coordinate, **R**.

2.3.3 Diabatic Representation

Equation 2.26 shows the limit of the adiabatic picture. This representation breaks down when the energy gap between the two states tends to zero, (V_j-$V_i \rightarrow 0$ resulting in $F_{ij} \rightarrow \infty$). In order to accurately represent the system it is preferable to switch to a diabatic representation.

In order to change to a diabatic representation we must replace the adiabatic coupling terms with a diabatic coupling matrix which contains the whole potential. The diabatic representation is the logical choice for systems containing significant non-adiabatic effects as it removes singularities created as V_j-$V_i \rightarrow 0$ creating a smooth and simple surface [23]. In this representation the Schrödinger equation is expressed:

$$\tilde{T}_N|\chi_i\rangle + \sum_j W_{ij}|\chi_j\rangle = i\hbar\frac{\partial}{\partial t}|\chi_i\rangle \tag{2.27}$$

where W_{ij} represents the potential matrix, coupling is represented by the off-diagonal elements. W_{ij} can be expressed as:

$$W_{ij} = \langle\phi_i|\tilde{H}_{el}|\phi_j\rangle \tag{2.28}$$

The diabatic states of a system are usually obtained from a unitary transformation of the adiabatic states. The orthogonal matrix, S transforms the operator from adiabatic to diabatic:

$$\Big(|\Phi_1\rangle|\Phi_2\rangle\Big) = S\Big(|\phi_1\rangle|\phi_2\rangle\Big) \tag{2.29}$$

In two state space the matrix, S can be written as a $\mathbf{R}$ dependent rotation:

$$S(R) = \begin{pmatrix} \cos\theta(R) & -\sin\theta(R) \\ \sin\theta(R) & -\cos\theta(R) \end{pmatrix} \tag{2.30}$$

where θ is the mixing angle between the two adiabatic states. From equation 2.30 we can write:

$$W^{11} = \langle\Phi_1|\hat{H}_{el}|\Phi_1\rangle = V_1\cos^2\theta + V_2\sin^2\theta \tag{2.31}$$

$$W^{22} = \langle\Phi_2|\hat{H}_{el}|\Phi_2\rangle = V_1\sin^2\theta + V_2\cos^2\theta \tag{2.32}$$

for the on-diagonal terms. For the off-diagonal terms we write:

$$W_{12} = \langle\Phi_1|\hat{H}_{el}|\Phi_2\rangle = (V_1 - V_2)\cos\theta\sin\theta \tag{2.33}$$

where $V_{1,2}$ are the adiabatic energies, W_{11} and W_{22} are the diabatic potential energies and W_{12} is the coupling.

2.4 The Vibronic Coupling Hamiltonian

In the following calculations a model Hamiltonian, the Vibronic Coupling Hamiltonian[2], is used where a set of N coupled states can be represented by a zeroth order Hamiltonian ($\mathrm{H}^{(0)}$), a diagonal matrix containing kinetic energy operators($\mathrm{W}^{(0)}$) and a set of diabatic coupling matrices($\mathrm{W}^{(1)}$):

$$\mathbf{H} = \mathbf{H^{(0)}} + \mathbf{W^{(0)}} + \mathbf{W^{(1)}} + ... \tag{2.34}$$

The zeroth order Hamiltonian, $H^{(0)}$, can be expressed using a harmonic oscillator around the Frank-Condon point. The zeroth order diagonal coupling matrix contains the energy of the electronic states at (Q_0), where ϕ is the diabatic electronic wavefunction.

$$W_{ii}^{(0)} = \langle \phi_i(Q_0) | H_{el} | \phi_j(Q_0) \rangle \tag{2.35}$$

where H_{el} is the standard clamped nucleus electronic Hamiltonian and ϕ_i the diabatic electronic functions. The following expressions describe the first order on-diagonal terms $W_{ii}^{(1)}$, the first order off diagonal terms $W_{ij}^{(1)}$ and the second order on diagonal terms $W_{ij}^{(2)}$

$$W_{ii}^{(1)} = \sum_{\alpha} \kappa_{\alpha}^{(i)} Q_{\alpha} \tag{2.36}$$

$$W_{ij}^{(1)} = \sum_{\alpha} \lambda_{\alpha}^{(i,j)} Q_{\alpha} \tag{2.37}$$

$$W_{ij}^{(2)} = \frac{1}{2} \sum_{\alpha,\beta} \gamma^{(i)} Q_{\alpha} Q_{\beta} \tag{2.38}$$

The use of symmetry arguments is very important in the VCHAM. Many expansion coefficients must be zero, only those where the product of the symmetries of the electronic states and the normal modes in question contain the totally symmetric irreducible repsentation are non-zero. This is shown in 2.39 for a first order off diagonal term (λ) for C_{2v} symmetry:

$$\Gamma_i \otimes \Gamma_{\alpha} \otimes \Gamma_j \supset A_1 \tag{2.39}$$

where Γ_i denotes the symmetry of the electronic state i and Γ_{α} denotes the symmetry of the normal vibrational mode α.

2.5 Symmetry and Group Theory

Understanding of the symmetry present in molcules is particuarly useful as it can be used to explain or predict a variety of chemical properties, for example its dipole moment and its allowed spectroscopic transitions [3, 4, 24]. For electronic structure, and other computational chemical, methods one can greatly reduce the ammount of computational expense by only calculating once for elements with the same symmetry.

Although a number of frameworks exist for the study of molecular symmetry the predominant framework is Group Theory [3, 24] (another major framework is the crystal systems used for bulk solids). Group Theory, as the name suggests, is a mathematical field which studies algebraic structures known as groups. It is a powerful method for analyzing systems (abstract as well as physical) in which symmetry is present.

One classifies a molecule according to group theory by assigning it a point group. A point group is a set of symmetry operations (a permutation of the atoms such that the molecule is transformed into an identical geometry to its initial geometry) for which at least one point remains fixed under all operations of the group. Figure 2.1 shows the symmetry operations present in a simple example molecule (H_20).

In addition to rotation axes and planes of symmetry, as demonstrated in figure 2.1 , the other symmetry operations are inversion centres, rotation-reflective axes (also known as a improper rotation axis) and the identity operation. An inversion centre (denoted I) is a point where each atom has an identical atom diametrically opposite this centre at an equal distance away from this centre. Rotation-reflective axes are an operation where a rotation about an axis followed by a reflection in a plane perpendicular to it results

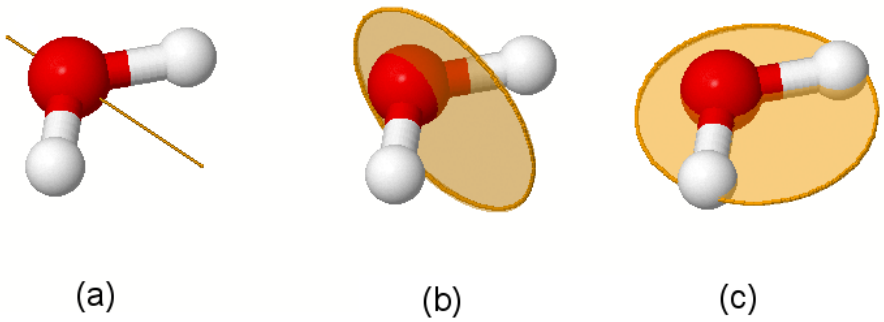

Fig. 2.1: A figure showing the symmetry operations present in the H_2O molecule. (a) shows the C_2 rotation axis (where the 2 indicates that the rotation is valid at $(\frac{360^\circ}{2})$, (b) shows a plane of symmetry (denoted σ, as does (c).

in a molecule indistinguishable to it. The identity operation consists of no change, being analogous to multiplying by unity, and is denoted (E).

Point groups can be expressed succinctly using character tables. Character tables consist of rows corresponding to irreducible representations and whose columns correspond to classes of group elements. An example character table for the C_{2v} point group in shown in table 2.1. When multiple planes of symmetry exist, as in both the previous figure 2.1 and in the character table 2.1 that follows, the different planes are differentiated from each other either by their relation to the principal axis or by using cartesian co-ordinates. The principal axis is the rotation axis with the highest order (n when the rotation is valid at $(\frac{360^\circ}{n})$.If the plane of symmetry is perpendicular to the principal axis it is termed horizontal and denoted by a subscript h (e.g. σ_h), when the plane of symmetry is parallel to the principal axis it is termed vertical and denoted by a subscript v (e.g. σ_v), and when the plane of symmetry is a vertical and also bisects the angle between two 2^{nd} order rotation axes

	E	$C_{2(z)}$	$\sigma_{v(xz)}$	$\sigma_{v(yz)}$
A1	1	1	1	1
A2	1	1	-1	-1
B1	1	-1	1	-1
B2	1	-1	-1	1

Table 2.1: The C_{2v} character table where $C_{2(z)}$ is a 2nd order rotation axis along the z axis, $\sigma_{v(xz)}$ is a plane of symmetry parallel to the principle axis.

perpendicular to the principal axis the plane is termed dihedral and denoted by a subscript d (e.g. σ_d). Cartersian co-ordinates can also be used to denote the plane in question, using subscripts x,y,z in order to denote the plane in question (e.g.σ_{xz}). These two forms are equivalent when convention is followed by defining the z-axis as that of the principle axis.

The character shown in table 2.1 is an example of an Abelian point group. Abelian point groups are commutative, that is the result of applying the group operation to two group elements is independent on their order, as shown in equation 2.40. When the point groups are not commutative, where a group operation performed on atleast two group elements are dependent on their order, they are termed non-abelian (non-commutative) point groups.

$$a \cdot b = b \cdot a \tag{2.40}$$

where a and b are group elements and $\cdot$ is a group operation.
Knowledge of a molecule's symmetry allows us to predict the type of transitions that may occur. This can be acieved by evaluation of the transition moment integral (equation 2.41) which for a transition to occur must be non-zero [25].

$$\int_{\infty}^{\infty} \psi_1 \mu \psi_2 d\tau \tag{2.41}$$

where psi_1 and psi_2 are the wavefunctions of the two states involved in the transition and μ is the transition moment operator. The transition is allowed if the direct product of the symmetries of the two states and the transition dipole operator spans the symmetry of the totally symmetric function (in the case of C_{2v} in figure 2.1 the totally symmetric function is An as it has a value of 1 with respect to each element). In practice one does not need to consider the transition moment integral, it is enough to know the symmetry of the transition moment operator. With this knowledge rules regarding which transitions result in a non-zero transition moment integral have been derived, termed selection rules [3, 25].

For electronic transitions the selection rules are that the total spin cannot change ($\delta S = 0$), that the change in total orbital angular momentum can be $\delta L = 0 or 1$ (but $L = 0$ to $L = 0$ is forbidden), that the change in the total angular momentum can be $\delta J = 0 or 1$ (but $J = 0$ to $J = 0$ is forbidden) and that the initial and final wavefunctions must change in parity (where the sum of the orbital angular momentum over all electrons, which can be even or odd).

For vibrational transitions the selection rule is such that vibration transitions are allowed as long as the change in vibration state is plus or minus a positive integer ($\delta v = \pm 1, 2, ...$ When $\delta v = 1$ this is called the fundamental vibration, those with larger $\delta v$are called overtones and only weakly allowed.

2.6 Jahn-Teller and Conical Intersections

The Jahn-Teller effect/theorem is an interesting effect whose definition greatly relies on group theory arguments. When the geometry for a non-linear molecule is described by a point group possesing degenerate irreducible rep-

resentations there always exists at least one non-totally symmetric vibration which makes electronically degenerate states unstable at this geometry [26]. This is particuarly apparent later in the thesis in the section on cyclobutadiene 4.3.

The Jahn-Teller effect gives rise to a conical intersection, but another effect can also give rise to conical intersections. The psuedo Jahn-Teller effect (or second order Jahn-Teller effect) arises when molecules with a non-degenerate ground electronic state and a degenerate excited state which is low lying, distortions arise that results in mixing of the ground and excited states which in turn lowers the ground-state energy.

In order for a molecule to have a Jahn-Teller CI it must fulfill the requirements of the Jahn-Teller theorum, specifically a molecular symmetry of C_3 or higher axis of rotation is required to generate degenerate irreducible representations of the point group and having a non-totally symmetric vibration of the same symmetry as the co-ordinates of the CI [27]. This type of conical intersection is also referred to as a symmetry allowed CI, in constract with with other two types of CIs namely accidental symmetry allowed and accidental same symmetry. Accicdental symmetry allowed CIs are between states with different point groups, and the elecronic states may or may not be degenerate when the symmetry is present. Accidental same symmetry CIs are between states with the same point group, as these cannot be anticipated using group theory arguments only recent advances in computational methods [27] have allowed these CIs to be investigated. Example plots of Conical Intersections are shown in figure 2.2.

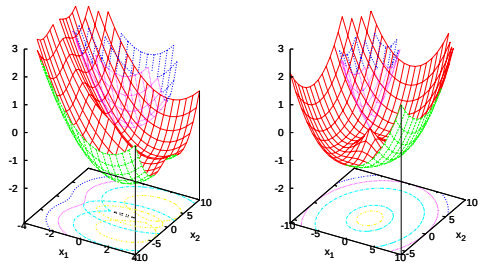

Fig. 2.2: The figure of the left shows an accidental symmetry allowed CI and right Jahn-Teller CI. Figure taken from [23].

2.7 Optimization

In order to select the parameters of the VCHAM potential energy surfaces are caculcated using electronic structure methods and the parameters are optimised to fit the calculated surfaces. This is an example of an optimisation problem, where one desires the best solution from all possible solutions. In the case of the VCHAM this is the set of parameters that yields the lowest root mean square deviation (RMSD) from the calculated surfaces.

This is typically achieved using local optimisation where one starts with an initial guess and then improves on the guess in an iterative process. In an early example, the Newton-Raphson method [28], where given a function $f(x)$, its derivative $f'(x)$ and a previous guess x_n the Newton-Raphson gives us the following expression for the first iteration (x_{n+1}):

$$x_{n+1} = x_n \frac{f(x_n)}{f'(x_n)} \tag{2.42}$$

Although an efficient optimisation technique the Newton-Raphson method has some deficiencies. In particular a poor initial guess can lead to non-convergence and in cases where the calculation of the function and its deriva-

tive are computationaly expensive the algorithm becomes inefficient. Numerous other methods for local optimisation exist which improve on the Newton-Raphson method with respect to its convergence problems such as the Simplex [29] and Conjugate-Gradient [30] methods both of which are used in the linear optimisation presented later in this thesis.

These methods however are still flawed, in that many problems have a large number of local minima. Local optimisers work by improving on an initial guess and are only able to find the local minima closest to the initial guess. Finding the global minima is a challenging problem and practically impossible for many situations. The brute force approach to solving a global optimization problem is a full space search, where $f(x)$ is solved for all possible values of x.

Numerous techniques have been developed in order to solve global optimisation approaches without resorting to full space searches. These can be classified as either Deterministic, Stochastic or Metaheurisitic. Deterministic approaches always return the same result for the same input, such as Branch and Bound methods [31] where the search space in separated into subsets (branches). In these Deterministic approaches if there is a subset A whose lower bound (of $f(x)$) is greater than the upper bound of subset B then subset A maybe discarded.

Stochastic methods use random variables as part of the optimisation problems, the classic example of which is the Monte Carlo [32] method where candidate solutions are generated at random over the seach space and then evaluated. Metaheurisitic methods [33] optimise a function by iteratively improving a candidate solution and often involve some sort of stochastic element.

2.8 Intramolecular Vibrational Relaxation

Intramolecular Vibrational Relaxation (IVR) is the process where vibrational energy localised in a particular mode is redistributed amongst the vibrational modes of a molecule. In early statistical theories IVR is assumed to be rapid and complete [34, 35]. More recent models [36–38] require coupling coupling matrix elements between the initially prepared state and all other vibrational states (although this is implemented in a variety of ways.)

Small molecules however do not relax statistically, as for example a study by Crim et. al. showed for bimolecular reactions of vibrationaly excited H_2O and HOD [39, 40].

Chapter 3

Computation and Methodology

The computational methods used in this thesis can be divided into two categories, time independent electronic structure methods and time dependent methods. The time independent electronic structure methods are used to describe the potential energy surface at a variety of nuclear geometries. Time dependent dynamic methods are used to determine the movement of a wavepacket on the potential energy surface calculated by the electronic structure methods.

Several electronic structure methods are used in this thesis. These methods are used sequentially in order to improve the result of the previous method. This is achieved by improving the treatment of electron-electron repulsion (correlation). As all of these methods optimise an initial guess, by using a simpler treatment of electron-electron repulsion initial convergence problems can be avoided.

The starting point for most *ab-initio* calculations is the Hartree-Fock (HF) method. The HF method treats the electronic interactions as an averaged field, hence the effects of electronic correlation are neglected. The next level of theory used in this thesis is complete active space self consistent field (CASSCF) theory which uses multiple excited electronic configurations in

determinants which account for electronic correlation statically. The complete active space with 2nd order perturbation (CASPT2/CASMP2) uses a second order perturbation to include dynamic correlation effects [4, 9, 41]. The dynamic calculations are performed using the multi configurational time dependent hartree (MCTDH) method [8, 23, 42]. This multiconfigurational approach implements correlation between the motion along the co-ordinates in question, which is not completely described in the mean field time dependent hartree (TDH) method.

3.1 Hartree-Fock Self Consistant Field (HF-SCF)

HF is the starting point for most ab-initio electronic structure methods. The HF method does not treat the electronic correlation. Each electron is considered to be moving in a field generated by (n-1) electrons. The HF Fock method is exact if the electron-electron repulsion term is ignored.

$$\hat{H}_e = \hat{T}_e + \hat{V}_{ne} + \hat{V}_{ee} + \hat{V}_{nn} \tag{3.1}$$

where $\hat{H}_e$ is the electronic Hamiltonian, $\hat{T}_e$ is the electronic kinetic energy operator, $\hat{V}_{ne}$ is the nuclear-electronic potential energy operator, $\hat{V}_{ee}$ is the electronic-electronic potential energy operator and $\hat{V}_{nn}$ is the nuclear-nuclear potential energy operator. By ignoring the electron-electron, $\hat{V}_{ee}$, term of the electronic hamiltonian 3.1 the wavefunction can be expressed as a simple product of one electron wavefunctions as shown in equation 3.2.

$$\Phi = \Phi_a(1)\Phi_b(2)\ldots\Phi_z(n) \tag{3.2}$$

where the first electron is described by Φ_a, the second by Φ_b and so on. This wavefunction (Φ) depends upon the co-ordinates of each electron and the positions of the nuclei. In order to fulfill the Pauli principle the product wavefunction must be expressed as a Slater determinant [4, 9, 41].

$$\Phi_{SD} = \frac{1}{\sqrt{N!}} \begin{vmatrix} \Phi_1(1) & \Phi_2(1) & \dots & \Phi_n(1) \\ \Phi_1(2) & \Phi_2(2) & \dots & \Phi_n(2) \\ \dots & \dots & \dots & \dots \\ \Phi_1(N) & \Phi_2(N) & \dots & \Phi_n(N) \end{vmatrix} \tag{3.3}$$

where $\Phi_n(N)$ represents a spin orbital for electron n. In order to determine the combination of spin orbitals which produces the best wavefunction one uses the variational theory to minimise the Rayleigh ratio of the determinant.

$$E_{HF} = \frac{\langle \Phi(R) | \hat{H} | \Phi(R) \rangle}{\langle \Phi(R) \mid \Phi(R) \rangle} \tag{3.4}$$

where E_{HF} is the energy of the ground state in nuclear configuration R. Performing this minimisation an expression for the optimal (HF) orbitals is obtained. This is written as:

$$F_i \Phi_a(1) = \epsilon_a \Phi_a(1) \tag{3.5}$$

$$F_i = h_i + \sum_a (J_a - k_a) \tag{3.6}$$

where F is the Fock operator, h is the core Hamiltonian, J is the coloumb operator and K is the exchange operator. For any electron Φ_a interacting with electron Φ_b these operators are defined as:

$$J_a \mid \Phi_b(2) \rangle = \langle \Phi_a(1) | \frac{1}{|r_a - r_b|} \mid \Phi_b(1) | \Phi_b(2) \rangle \tag{3.7}$$

$$K_a \mid \Phi_b(2)\rangle = \langle \Phi_a(1)| \frac{1}{|r_a - r_b|} |\Phi_b(1)\rangle \Phi_a(2)\rangle \tag{3.8}$$

In order to solve equation 3.5, which would be computationally complex for molecular systems. Roothan and Hall [43] suggested expanding the spin orbitals in a known basis set with the form:

$$\Phi_a = \sum_{\alpha} c_\alpha \chi_\alpha \tag{3.9}$$

where c_α are the coefficients which are calculated using the self consistent field (SCF) method and χ_α are the basis functions. The linear combination of these basis functions describe the wavefunction under consideration, which is represented as a vector containing the coefficients of the basis functions. These functions are typically used in sets designed to be able to represent the molcular orbitals. The SCF method changes the nature of the problem to the calculation of coefficients. Using equation 3.5 and 3.9 we can now write:

$$F_i \sum_{j=1}^{m} c_{j\alpha} \chi_\alpha(1) = \epsilon_a \sum_{j=1}^{m} c_{j\alpha} \chi_\alpha(1) \tag{3.10}$$

By multiplying by $\chi_j(1)$ and integrating over the spin space we can write:

$$\mathbf{FC} = \mathbf{SC}\epsilon \tag{3.11}$$

where $\mathbf{F}$ is the Fock matrix $\langle \chi_a | F_i | \chi_b \rangle$, $\mathbf{S}$ is the overlap matrix $\langle \chi_a \mid \chi_b \rangle$ and $\mathbf{C}$ is a matrix containing the spin orbital coeffiecients. This cannot be solved directly because the matrix elements of the Fock matrix involve integrals over the Coulomb and exchange operators which are dependent on the spatial wavefunctions. It can be solved by taking an initial guess of the coefficients (equation 3.9). These are then evaluated using equation 3.12.

$$\det|\mathbf{F} - \epsilon_a \mathbf{S}| = 0 \tag{3.12}$$

By solving equation 3.12 we receive new values for the coefficients. This continues in an iterative manner until a predefined convergence criterion is reached.

3.2 Basis Sets

The results can be improved, energetically, by increasing the size of the basis set. A basis set is a set of functions used to describe the molecular orbitals, although with a very small system (atoms and diatomics) the Hartree-Fock equations may be solved by mapping the orbitals on a grid (termed numerical Hartree-Fock) [9]. In practice all calculations use a basis set expansion to describe the molecular orbitals as a set of known functions. Although in principle any type of function may be used (exponential, Gaussian, polynomial etc.) typically exponential and gaussian are used. Each molecular orbital is expanded in terms of the basis functions (also referred to as atomic orbitals, the method itself called a linear combination of atomic orbitals) as shown in fig 3.13.

$$\phi_i = \sum_{\alpha}^{M} c_{\alpha,i}\chi_\alpha \tag{3.13}$$

where phi_i is the molecular orbital i, $c_{\alpha,i}$ is the coefficient for the basis function (atomic orbital) α and molecular orbital i, and χ_α is the basis function (atomic orbital) α. The first type of basis function used extensively were Slater Type Orbitals (STOs) [44] which are functions that decay exponentially with distance from the nuclei. Although these functions are well suited

to describe molecular orbitals the calculation of multi-centred two-electron integrals is computationaly expensive.

It was later discovered that STOs could be approximated as linear combinations of Gaussian functions [45] , which overcomes the expense of the STO as it is much easier to calculate the two-electron integrals with Gaussian functions. It is significantly easier to calculate to electron integrals with Gaussian Type Orbitals (GTO) as the product of two Gaussian functions, with different positions and exponents, can be written as a single Gaussian function located between the two original functions.

Minimal basis sets are able to represent all the electrons on each atom, the most common of which is the STO-nG series where STO indicates Slater Type Orbitals and n represents the number of primitive Gaussian functions comprising a single basis function. The majority of research is performed with larger basis sets, for example split-valence basis sets.

As it is the valence electrons that primarily take part in molecular bonding it is common to represent valence electrons with a linear combination of more than one basis function (GTOs, which are a linear combination of primitive Gaussian functions.) These different orbitals have different spatial magnitudes and the combination allows the wavefunction to extend and adapt to the molecular environment. As minimal basis sets are fixed they are unable to adjust to different molcular environments resulting in inaccuracies. Basis sets where multiple basis functions are used to describe each valence atomic orbital are referred to as double-zeta, triple-zeta, quadruple-zeta etc.

In this paper basis sets created by the group of John Pople [9, 45] are used, typically referred to as Pople basis sets. These are descibed in A-BCDEg notation, where A represents the number of primitive Gaussians comprising each core atomic orbital basis function. B, C, D, and E show that the valence

orbitals are composed of four basis functions each, the first consisting of B primitive gaussian functions, the second D primitive gaussian functions and so on. In this case this is a quadruple-zeta split-valence basis set, in the case of a double-zeta split-valence basis set the D and E would be omitted.
Another common addition to basis sets, minimal and split-valence alike, is the use of polarization functions to describe the polarization of the orbitals. In the case of a s type orbital a p type orbital would be added to describe the polarization, for a p type orbital a d type orbital would be added and so on. In the case of Pople basis sets an asterisk * is used to denoted the addition of polarization functions, a double asterisk ** indicates that polarization functions are also added to the light atoms (hydrogens).
In order to obtain a more accurate result, particularly in terms of its energetics, the electronic correlation must be calculated more accurately than in the HF method detailed above. The following sections detail some approaches towards the inclusion of electronic correlation.

3.3 Configuration Interaction

The simplest to understand method for including the the electronic correlation is the Configuration Interaction (CI) Method. This method uses a linear combination of slater determinants (configurations) to describe the wavefunction and mixing (interaction) of different electronic states, giving rise to the name Configuration Interaction. As CI goes beyond HF it is often described, like the electronic structure methods that follow, as a post Hartree Fock method [9].
In order to include the electron correlation the CI method uses a variational wavefunction defined as a linear combination of Configuration State Func-

tions (CSFs). A CSF is a symmetry adapted linear combination of slater determinants and is defined in equation 3.14 , with the CI wavefunction defined in equation 3.14

$$\psi = \sum_i c_i \Phi_i \tag{3.14}$$

where *psi* is configuration state function, c are coefficients and Φ is a slater determinant.

$$\Psi = \sum_k c_k \psi_k \tag{3.15}$$

where c are coefficients and ψ are configuration state function as described in 3.14. The CSFs are built from spin orbitals, so the wavefunction can also be expressed as in terms of spin orbitals as shown in equation 3.16.

$$\Psi = \sum_{k=0} c_k \phi_k \tag{3.16}$$

where Φ is the wavefunction, c is a coefficient and ϕ is configuration state function. When the expansion in equation 3.16 includes all CSFs of the appropriate symmetry this is termed a full configuration interaction procedure. A full CI solves the Schrödinger equation exactly (within the limits of the basis set).

This is a constrained optimization, where the energy is minimised under the constraint that the total CI wavefunction is normalised. By introducing a lagrange multiplier [9] we can rewrite equation 3.15 as equation 3.17.

$$L = \langle \Psi_{CI} | \hat{H} | \Psi_{CI} \rangle - \lambda [\langle \Psi_{CI} | \Psi_{CI} \rangle - 1] \tag{3.17}$$

where L is the Lagrange function, Ψ_{CI} is the CI wavefunction, $\hat{H}$ and λ is

the Lagrange multiplier. Theses two terms (left hand and right hand terms in equation 3.17 can be written in terms of determinants (see equation 3.14) as follows.

$$\langle \Psi_{CI}|\hat{H}|\Psi_{CI}\rangle = \sum_{i=0}\sum_{j=0} a_i a_j \langle \Phi_i|\hat{H}|\Phi_j\rangle = \sum_{i=0} a_i^2 E_i + \sum_{i=0}\sum_{j=0} a_i a_j \langle \Phi_i|\hat{H}|\Phi_j\rangle \tag{3.18}$$

$$\lambda[\langle \Psi_{CI}|\Psi_{CI}\rangle - 1] = \sum_{i=0}\sum_{j=0} a_i a_j \langle \Phi_i|\Phi_j\rangle = \sum_{i=0} a_i^2 \langle \Phi_i|\Phi_j\rangle = \sum_{i=0} a_i^2 \tag{3.19}$$

The diagonal elements of the Hamiltonian operator in equation 3.18 are the energies of the corresponding determinants. As the determinants are built from orthogonal molecular orbitals the overlap elements between different determinants are zero. The variational procedure can then be used to set all the derivatives of the lagrange function 3.17 ,with respect to the a_i expansion coefficients, equal to zero, as shown in equations 3.20,3.21 and 3.22.

$$\frac{\delta L}{\delta a_i} = \sum_j a_i \langle \Phi_j|\hat{H}\Phi_i\rangle - 2\lambda a_i = 0 \tag{3.20}$$

$$a_i(\langle \Phi_i|\hat{H}|\Phi_j\rangle - \lambda) + \sum_{j\neq i} a_j \langle \Phi_i|\hat{H}|\Phi_j\rangle = 0 \tag{3.21}$$

$$a_i(E_i - \lambda) + \sum_{j\neq i} a_j \langle \Phi_i|\hat{H}|\Phi_j\rangle = 0 \tag{3.22}$$

As there is one equation, as expressed in equation 3.22, for each i the variational problem becomes one of solving a set of CI secular equations. Where $H_{ij} = \langle \Phi_i|\hat{H}|\Phi_j\rangle$ one can express this problem in matrix form, as shown in

equation 3.23.

$$H(t) = \begin{pmatrix} H_{00}-E & H_{01} & ... & H_{0j} & ... \\ H_{10} & H_{11}-E & ... & H_{1j} & ... \\ ... & ... & ... & ... & ... \\ H_{j0} & ... & ... & H_{jj}-E & ... \\ ... & ... & ... & ... & ... \end{pmatrix} \begin{pmatrix} a_0 \\ a_1 \\ ... \\ a_j \\ ... \end{pmatrix} = \begin{pmatrix} 0 \\ 0 \\ ... \\ 0 \\ ... \end{pmatrix} \tag{3.23}$$

Solving the secular equation is equivalent to diagonalising the CI matrix. The CI energy as the lowest eigenvalue of the CI matrix and the corresponding eigenvector contains the a_i coefficients in front determinants in equation 3.14. The computational effort required when using the CI method is proportional to the size of the CI matrix. Even for small systems, e.g. H_2O with a 6-31G* basis set, the CI matrix is vast. With 10 electroncs and 38 spin orbitals (H_2O example) there are $k_{10,n}$ ways of distributing the electrons in the 28 empty orbitals. Thus the number of excited states for a given excitation level is $k_{10,n} \cdot k_{28,n}$. The total number of excited determinants will be a sum over 10 such terms (analogous to each electron being excited to each possible excited state), which is equivalent to $k_{38,10}$ the total number of ways 10 electrons can be distributed in 38 orbitals. This is expressed in equation 3.24 and in a more general form in equation 3.25.

$$NumberofSDs = \sum_{n=0}^{10} k_{10,n} \cdot k_{28,n} = \frac{38!}{10!(38-10)!} \tag{3.24}$$

$$NumberofCSFs = \frac{M!(M+1)!}{(\frac{N}{2})!\,(\frac{N}{2}+1)!(M-\frac{N}{2})!(M-\frac{N}{2}+1)!} \tag{3.25}$$

So for the H_2O example, with the basis set 6-31G* basis set there are $20x10^6$ CSFs. This factorial groth of the number of CSFs makes the CI method

unfeasibile for any sizeable molecule. The following sections go on to detail alternative methods to include electronic correlation, but without the expenses of a CI calculation./

3.4 Complete Active Space Self Consistant Field (CASSCF)

By using a mean field approach the HF method fails to take into account instantaneous electron-electron interactions and therefore is unable to describe the numerous quantum effects that rely on an accurate description of the electronic distribution, As discussed in the previous section the HF method yields a set of spin orbitals forming a Slater determinant in which the lowest n orbital are occupied by $2n$ electrons. We can describe the system with many more determinants by occupying the virtual orbitals.

By considering multiple electronic configurations, using the virtual orbitals as well as the ground state configuration, we are able to improve our description of the electronic correlation. The multi configurational self consistent field method (MCSCF) optimises both the co-efficients in front of the determinants and the spin orbitals used for constructing the determinants. This is analogous to performing a configuration interaction calculation but only over a limited number of configurations.

The major problem with the MCSCF method is selecting the necessary configurations for an accuate description of the property(ies) of interest. In this thesis this problem is alleviated by using the complete active space self consistent field (CASSCF) method [9]. In the CASSCF method the configurations are selected by partitioning the molecular orbitals into active, core and virtual orbitals. Active orbitals are typically some of the highest occupied and

lowest unoccupied molecular orbitals from a previous HF calculation. Core orbitals remain doubly occupied and virtual orbitals remain unoccupied in all determinants.

The active molecular orbitals are selected by hand, by considering all the orbitals likely to change significantly while exploring the problem at hand. In the case of the research presented in this thesis, where many points are required on the excited state potential energy surface, the orbitals occupied in the excited states of interest and where the distortion from the ground state equilibrium geometry changes the orbital dramatically.

3.5 Complete Active Space with 2nd Order Perturbation (CASPT2)

The multi reference nature of CASSCF allows it to take into account static correlation, however to improve the description of the system further dynamic correlation is required. One method for including this is the use a perturbative method such as complete active space with the 2nd order perturbation (CASPT2) [46]. The basis of the CASPT2 method is the division of the hamiltonian into a zero order part ($\hat{H}_0$) and a perturbation ($\hat{V}$).

$$\hat{H} = \hat{H}_0 + \lambda\hat{(V)} \tag{3.26}$$

where λ is the perturbation factor. In CASPT2 the zero order Hamiltonian $\hat{H}_0$ is the CASSCF hamiltonian. Substituting this into the time independent Schrödinger equation (TISE) we obtain:

$$\hat{H} \mid \Phi_I\rangle = (\hat{H}_0 + \lambda\hat{V}) \mid \Phi_i\rangle = \epsilon_i \mid \Phi_i\rangle \tag{3.27}$$

where Φ_I is the CASPT2 wavefunction and Φ_i is the CASSCF wavefunction. We know the eigenfunction and the eigenvalue of H_0 is:

$$\hat{H}_0 \mid \Phi_i^{(0)}\rangle = W_i^a \mid \Phi_i^{(a)}\rangle \tag{3.28}$$

In order to converge on the full Hamiltonian, $\hat{H}$, we must systematically improve the eigenvalues of $\hat{H}_0$. In order to achieve this we expand the exact eigenfunctions and eigenvalues in a Taylor series in λ which gives us the following:

$$\epsilon_i = W_n^{(0)} + \lambda^2 W^{(1)} + \ldots \tag{3.29}$$

$$|\Phi_i\rangle = |\Psi_i^{(0)}\rangle + \lambda|\Psi_i^{(1)}\rangle + \lambda^{(2)}|\Psi_i^{(2)}\rangle + \ldots \tag{3.30}$$

where ϵ_i is the orbital energy for orbital i, W_i^n is the nth order correction to the energy, Ψ_i^n is the nth order correction to the wavefunction. With the expansions in equation 3.29 and 3.30 the TISE 3.27 becomes:

$$(H_0 + \lambda V)(|\Psi_i^{(0)}\rangle + \lambda|\Psi^{(1)}\rangle + \ldots) = (W_i^0 + \lambda W_i^{(1)} + \ldots)(|\Psi_i^{(0)}\rangle + \lambda|\Psi_i^{(1)}\rangle + \ldots \tag{3.31}$$

As this holds for any value of λ we can collect terms with the same power of λ to give:

$$\lambda^0 : H_0|\Psi_i^{(0)}\rangle = W_i^{(0)}|\Psi_i^{(0)}\rangle \tag{3.32}$$

$$\lambda^1 : H_0|\Psi_i^{(1)}\rangle + V|\Psi_i^{(0)}\rangle = W_i^{(0)}|\Psi_i^{(1)}\rangle + W_i^{(0)}|\Psi_i^{(0)}\rangle \tag{3.33}$$

$$\lambda^2 : H_0|\Psi_i^{(2)}\rangle + V|\Psi_i^{(1)}\rangle = W_i^{(0)}|\Psi_i^{(2)}\rangle + W_i^{(1)}|\Psi_i^{(1)}\rangle + W_i^{(2)}|\Psi_i^{(0)}\rangle \tag{3.34}$$

$$\lambda^n : H_0|\Psi_i^{(n)}\rangle + V|\Psi_i^{(n-1)}\rangle = \sum_{j=0}^{n} W_i^{(j)}|\Psi_j^{(n-j)}\rangle \tag{3.35}$$

The zero order equation is just the Schrödinger equation for the unperturbed problem. The first order equation contains just two unknowns, the first order correction to the energy, W, and the first order correction to the wavefunction. The nth order energy correction, W^n, can be calculated by multiplying from the left by Φ_0 and integrating using the turnover rule equation 3.36 to give us equation 3.37.

$$\langle \Phi_0 | H_0 | \Phi_i \rangle = \langle \Phi_i | H_0 | \Phi_0 \rangle \tag{3.36}$$

$$W_n = \langle \Phi_0 | V | \Phi_{(n-1)} \rangle \tag{3.37}$$

We are still dealing with undetermined quantities, energy and wavefunction corrections at each order. However using the complete set of functions generated by the unperturbed Schrödinger equation we can expand the first order correction in these functions. For the λ^1 equation 3.33 becomes:

$$|\Psi_i^{(1)}\rangle = \sum_n c_n^i |n\rangle \tag{3.38}$$

We can then multiply 3.33 by $\langle n|$ and using the knowledge that the zero order wave functions are orthogonal we can derive:

$$(W_i^{(0)} - W_n^{(0)}) \langle n | \Psi_i^{(1)} \rangle = \langle n | V | \Psi_i^0 \rangle \tag{3.39}$$

and using $|\Psi_i^{(i)} = \sum_n |n\rangle \langle n \mid \Psi_i^{(1)}\rangle$ with equation 3.37 where $n = 1$ we derive

$$W_i^2 = \sum_n \langle \Psi_i^0 | V | n \rangle \langle n \mid \Psi_i^{(1)} \rangle \tag{3.40}$$

and by finally using equation 3.39 we arrive at a term for the 2nd order energy correction:

$$W_i^{(2)} = \frac{\sum_n |\langle \Psi_i^0 | V | n \rangle|^2}{W_i^{(0)} - W_n^{(0)}} \tag{3.41}$$

The formulae for higher corrections become increasingly complex. Corrections can be expressed in terms of matrix elements of the pertubation operator over the energies. The CASPT2 method only uses a second order perturbation. This allows us to calculate energies in a molecular system very accurately, particularly where the CASSCF worked well.

CASPT2 is not without its difficulties however, problems can arise when two electronic states have very similar energies or when intruder states occur. Intruder states arise when the energy of a pertubation is of a similar magnitude to the energy associated with the zero order wavefunction. To solve these problems Roos et al. [47] devised a method of shifting the energy levels and recalculated without this interference. In an energy shift calculation the Hamiltonian takes the form:

$$\hat{H}_0 = \hat{H}_0 + \zeta P_e \tag{3.42}$$

where ζ is a small positive shift value and P_e is a projection operator on the interacting space. This succesfully removes the intruder states and allows calculation of almost degenerate levels without shifting the relative energy of the states.

3.6 Multi-Configurational Time Dependent Hartree (MCTDH)

Molecular dynamics methods were first developed for the study of hard spheres [48, 49] in the late 1950s. This and other early work [50] used classical particles swarming over a potential energy surface. These studies were able to reproduce much useful information, but they were not without inaccuracies. In order to account for the inaccuracies semi-classical methods were developed. One study of note was the use of Gaussian wavepackets by Heller [51] which is commonly used in modern methods.

The first full quantum dynamics simulation was reported by McCullough and Wyatt [52] in 1969 on the H+H_2 exchange reaction. Since then there have been numerous important developments for example the introduction of grid based methods such as the Fast Fourier Transform (FFT) method by Koslov [53] and the Discrete Variational Representation (DVR) [54].

The normal approach for solving the TDSE using a propagating wavepacket is to express the wavefunction in a time independent basis with time dependent co-efficients:

$$\Psi(Q_1,\ldots,Q_f,t) = \sum_{j_1=1}^{N_1}\cdots\sum_{j_1=1}^{N_1}(c_{j_1},\ldots,c_{j_f}(t)\prod_{k=1}^{f}\chi_{j_k}^{(k)}(Q_k) \tag{3.43}$$

where f specifies the number of degrees of freedom, $Q_1,\ldots,Q_f$ are normal mode nuclear coordinates, $c_{j_1},\ldots,c_{j_f}$ are the time dependent coefficients and $\chi_{j_k}^{(k)}$ are the time independent basis functions and N_f is the number of basis functions used for the f^{th} degree of freedom (DOF). The disadvantage of this approach is that the computational effort grows exponentially with the number of DOF. The number of coefficients for a calculation with N basis functions and f degrees of freedom is N^f.

For large systems this is not practical and approximate methods for solving the time dependent Schrödinger equation must be implemented. An example of this is the time dependent hartree (TDH) approach. In this approximation the basis functions are time dependent, unlike those in the standard method, giving us the following expression for the wavefunction.

$$\Psi(Q_1, \ldots, Q_f, t) = a(t)\varphi_1(Q_1, t) \ldots \varphi_f(Q_f, t) \tag{3.44}$$

where $a(t)$ is a time dependent complex number and φ are one dimensional functions. The product $\varphi_1\varphi_2 \ldots$ is called a Hartree product. The time independent basis functions optimally describe the evolving wavepacket but, as in HF theory, each DOF is only affected by the other evolving DOF in an averaged fashion. The lack of correlation in the TDH approach leads to poor performance, particularly where the PES changes significantly over the width of the wavepacket. In the way MCSCF uses multiple configurations to add correlation to HF calculations the same technique can be used to add correlation to TDH calculations.

3.6.1 General Formulation

The multi configurational time dependent hartree (MCTDH) method uses this concept, giving us an expression for the wavefunction as a linear combination of Hartree products:

$$\Psi(Q_1, \ldots, Q_f, t) = \sum_{j_1=1}^{n_1} \ldots \sum_{j_f=1}^{n_f} A_{j_1, \ldots, j_f}(t) \prod \varphi_{j_k}^{(k)}(Q_k, t) \tag{3.45}$$

$$\Psi(Q_1, \ldots, Q_f, t) = \sum_j A_j \Phi_j \tag{3.46}$$

where $A_{j_1},\ldots,_{j_f}$ denotes the MCTDH expansion coefficients and $\varphi_{j_k}^{(k)}$ are the expansion functions for each k DOF, referred to as single particle functions (SPF). The number of configurations represented in the wavefunction is n_k^f by setting the number of configurations to 1 equation 3.45 becomes the TDH wavefunction equation 3.46 defines the composite index and Φ is the Hartree product.

Using the Dirac-Frenkel variational principle and equation 3.45 one can obtain a set of coupled equations of motion. Equation 3.47 shows the equation for the expansion coefficients and equation 3.48 shows the equations for each set of SPFs:

$$iA_j = \sum_i KA_i \tag{3.47}$$

$$i\underline{\varphi^{(k)}} = (1-P^k)(\underline{\underline{\rho^{(p)}}})^{-1}\underline{\underline{H^{(k)}}}\,\underline{\varphi^{(k)}} \tag{3.48}$$

A_j uses a composite index representing $A_{j_1},\ldots,A_{j_f}$, $\underline{\underline{\rho^{(p)}}}$ is the density matrix, $P^{(k)}$ is a projector onto the SPF space and $H^{(k)}$ is the mean field operator. The matrix K is the Hamiltonian operator in the Hartree basis:

$$K = \langle\Phi_J|H|\Phi_I\rangle \tag{3.49}$$

The projection operator $(1-P^k)$ where:

$$P^k = |\varphi_j^{(k)}\rangle\langle\varphi_j^{(k)}| \tag{3.50}$$

ensures that the time derivative of the SPF retains orthogonality. When the basis is complete, where $1-P=0$, the SPF become time independent and the equations of motion are indentical to the standard method. $H^{(k)}$, the mean field operator, and $\rho^{(k)}$, the density matrix are expressed:

$$\langle H\rangle_{ab}^{(k)} = \langle \Psi_a^{(k)}|H|\Psi_b^{(k)}\rangle \tag{3.51}$$

$$\rho_{ab}^{(k)} = \langle \Psi_a^{(k)} \mid \Psi_b^{(k)}\rangle \tag{3.52}$$

where the single hole functions $\Psi_a^{(k)}$ ignore the SPF of the k^{th} mode, $\varphi_a^{(k)}$ and the integration is over all the DOF except k. The mean field operators represent the correclation between two different sets of SPFs (J and L).

3.6.2 Memory requirements

As mentioned previously the standard method expressed in 3.43 has a large scaling problem (N^f coefficients where f is the number of DOF and N the number of basis function). This leads to large memory requirements with even relatively small systems. The memory requirements for the MCTDH method however can be expressed as:

$$\text{memory } n^p + pnN^d \tag{3.53}$$

where n is the number of SPF, p the number of particles, N is the number of time independent basis functions required to describe the single particle function. The first term in the expression is the number of A coefficients and the second is the representation of the SPF using a set of DVR functions written:

$$\varphi_j^{(k)}(Q_k) = \sum_{k=1}^{N_k} a_{k_j}^{(k)} \chi_k^{(k)}(Q_k) \tag{3.54}$$

Although there is still exponential scaling $n < N$ and $p < d$ resulting in a significantly reduced scaling problem.

3.6.3 DVR Functions

The DVR is a widely used grid based representation for wavefunctions and operators. This provides an alternative to the problem of solving complex integrals [54–56] which in a numerical calulation is often challenging. The time independent basis of the DVR functions exist in various forms such as harmonic, Legendre and exponential. In order to solve the equations of motion (3.47 and 3.48) we must evaluate the elements of the Hamiltonian matrix k:

$$\langle \varphi_{j_1}^{(1,2,\ldots)} \ldots \varphi_{j_1}^{(1,2,\ldots)} | H | \varphi_{j_1}^{(1,2,\ldots)} \ldots \varphi_{j_1}^{(1,2,\ldots)} \rangle = \langle \varphi_{j_1}^{(1,2,\ldots)} \ldots \varphi_{j_1}^{(1,2,\ldots)} | T+V | \varphi_{j_1}^{(1,2,\ldots)} \ldots \varphi_{j_1}^{(1,2,\ldots)} \rangle \tag{3.55}$$

A set of DVR functions ($\chi^{(v)}(q_v)$) along coordinate q_v has a diagonal position representation, therefore:

$$\langle \chi_i^{(v)} | q_v | \chi_j^{(v)} \rangle = q_v^{(v)} \delta_{ij} \tag{3.56}$$

The eigenvalue of this matrix provide the grid points related to the DVR functions. If there are sufficient grid points to describe the wavepacket the potential energy operator can be considered diagonal in this basis. The kinetic operator usually acts on one coordinate and therefore matrix elements are evaluated in the finite bases representation (FBR). This can be transformed using the FBR-DVR transformation, details of which can be found in reference [8]

3.6.4 Autocorrelation Functions and Calculation of Spectra

Spectra are calculated using an autocorrelation function calculated by a quantum dynamics simulation. A time dependent autocorrelation function, C(t) indicates how a wavepacket overlaps its initial value.

$$C(t) = \langle \Psi(0) \mid \Psi(t) \rangle \tag{3.57}$$

The absorption spectrum, $I(\omega)$ for a given molecule us generated by a Fourier transform of $C(t)$ to the frequency domain.

$$I(\omega) \int_{-\infty}^{\infty} C(t) e^{-i\omega t} dt \tag{3.58}$$

The auto correlation function is usually modified before performing FT in order to avoid problems during the FT and to add lorentzian broadening. Firstly the autocorrelation function is multiplied by $\cos^2(\frac{n\pi t}{2T})$ where n = 1,2,3... and T denotes the final time (plus one time step), in order to reduce artifacts created by overshooting of the fourier sum at a discontinuity jump. Secondly in order to add Lorentzian broadening to model spectroscopic resolution, or any other type of damping the autocorrelation function is multiplied by $\exp(\frac{-|t|}{\tau^i})$ where τ is the damping time [8].

3.6.5 Geometry Optimization

Geometry optimization, or energy minimization (with respect to optimizing the geometry to find the lowest energy), methods are used to compute the equilibrium geometry of molecules. In the course of this thesis geometry optimizations are performed at numerous points before performing other calculations discussed above using the calculated geometry. The equilibrium

geometry corresponds to the global minimum on the potential energy surface of the molecule in question, other geometries can also be calculated corresponding to reactive intermediates and transition states (local minima and maxima respectively).

The optimization techniques discussed in section 2.7 are frequently used to optimise geometries. First order approaches, those that only require calculation of the first order analytic derivatives, such as the Newton-Raphson method are common as are those in extended versions (termed Quasi-Newton methods, such as Conjugate-Gradient) which can be considered an intermediary method between first and second order approaches. Second order approaches, requiring second order derivatives, are able to reach convergence using less iterations than first order methods [57] but due to the fourth/fifth order scaling of the computational expense with system size second order methods quickly become impractical.

In this thesis the geometry optimization method used is the Berny algorithm [58, 59] in redundant internal co-ordinates [60, 61] as implemented in the GAUSSIAN 03 [62] program. This uses Newton-Raphson optimization steps but in order to avoid the convergence difficulties the Berny algorithm uses the rational functional model [63] and the trust radius model [57] in order to control Newton-Raphson step sizes. The number of iterations required to reach convergence is also reduced compared to true first order methods using a least-squares minimisation scheme, namely direct inversion in the iterative subspace [64]

Chapter 4

Genetic Algorithm

4.1 Introduction

The development of a genetic algorithm to fit model potential energy surfaces to ab-initio calculated surfaces was prompted by difficulties in the fitting of the toluene model surfaces. In order for the model surface fitting to reach a satisfactory conclusion certain co-efficients of the model required initial values determined by hand. This time consuming approach was not desireable and an automatic approach was required.

The coefficients of the model surface can be determined by evaulating the derivatives of the surfaces at Q_0. A more appropriate method is to calculate the parameters that best fit the model surfaces to the ab-initio calculated surfaces. Previously this has been performed by calculating points along the various normal modes and optimizing the parameters [42, 65] by optimizing the least-squares fit function

$$F = \Sigma\omega_i(V_i^{calc} - V_i^{mod})^2 \tag{4.1}$$

Where V_i^{calc} are the ab-initio calulated potential energies and V_i^{mod} are the model potential energies at point i and ω_i is a weighting function which can be used to preferentialy fit the reference points of lower energy.

Numerous algorithms have been used for optimizations such as this, for example Newton's method (or the Newton-Raphson method) [28] and the Conjugate Gradient [66] method. Newton's method is a well known algorithm for finding the roots of equations, it can also be used to find local maxima and minima of functions, as these are the roots of the derivative function. Provided that the function in question is twice differentiable and the initial guess x_0 is close enough the stationary point x then the iterative sequence(x_n) is defined as:

$$x_{n+1} = x_n - \frac{f'(x_n)}{f''(x_n)}\,, n \geq 0 \tag{4.2}$$

Although powerful Newton's method has numerous short comings. The requirement for the direct calculation of the derivative which is often time consuming and in our case the difficulties reaching convergence make it quite impractical. A more practical alternative is the conjugate gradient method, which has been used for much of my own work. If we define the optimization problem as $Ax = b$ where x is our soloution and A is a symmetric, positive-definite and real $n * n$ matrix the we define the iterative sequence as:

$$x_{n+1} = x_n + \alpha_{n+1} p_{n+1} \tag{4.3}$$

$$p_{n+1} = r_n - \sum_{i \leq n} \frac{p_i^T A r_n}{p_i^T A p_i} \, p_i \tag{4.4}$$

$$\alpha_n + 1 = \frac{p_{n+1}^T r_k}{p_{n+1}^T A p_{k+1}} \tag{4.5}$$

Where p_n are our conjugate vectors and r_n is the residual at the n^th step. This method has numerous benefits in terms of ease of convergence and in the size and complexity of the systems it is able to handle. However both of these methods are still limited to finding the local minima closest to their initial value and are hence termed local optimizers. In order to determine the optimal fit, the global minimum, a global optimizer is required. Only a full space search, where one generates every possible set of parameters and evaluates their fitness, is able to determine the global minmum with certainty. This is a computationally expensive route, as evaluating the fitness requires calculating the deviation from the ab-initio reference points. Solving the model for each reference point is time consuming, and in a full space search it would need to be calculated for every possible value of each parameter. For a simple model of 10 parameters, for example, taking each parameter as a double precision real number (2048 possible values of the exponent and 4,294,927,296 possible values of the fraction) and limiting each value to a sensible range (-4 to 4 eV) would give us $3.006 * 10^{10}$ possible values for each parameter. This is prohibitively expensive and has promoted the creation of numerous techniques which explore the full search space and locate probable global minima. For geometry optimization problems global optimization algorithms are used routinely for clusters [67, 68], Nano particles [69], crystal structures [70] and biomolecules [71]. The majority of global optimization methods used for geometry optimization incorporate random elements and are termed stochastic optimizers. These algorithms deliberately introduce randomness into the search process in order to reduce the sensitiv-

ity of small modelling errors (which can cause local optimization algorithms to converge to a local minima) and to provide a means of moving away from a local minimum. Examples of global optimizers include Monte-Carlo optimization [32, 72], basin hopping [73, 74], simulated annealing [74, 75] and stochastic tunneling [76]. Monte-Carlo methods are quite varied, being the oldest global optimization technique, but follow a simple pattern where solutions are randomly generated and their fitness tested. Variations include Monte-Carlo with local optimization where local optimization is performed on each solution allowing it to reach the bottom of the local minima, greatly enhancing the area searched.

Basin hopping is another variation on the Monte-Carlo method where the search space is transformed into a collection of basins (analogous with local minima) by lowering the barriers between local minima and explores them by hopping between them. The 'hopping' is determined by random Monte-Carlo moves and then evaluated. Simulated annealing is a method analogous to annealing in metallurgy, where heating and controlled cooling of a material is used to increase the size of its crystals and reduce their defects. Each iteration of the simulated annealing method replaces the current solution by a random nearby solution, chosen with a probability that depends on its difference from a global parameter T (temperature), that is slowly decreased during the process.

Simulated annealing is especially effective when only an acceptable solution is required, rather than the global minima. As the temperature lowers the solution becomes trapped in a minima, this can be overcome using stochastic tunneling, which acts in much the same way as basin hopping effects Monte-Carlo optimization. By lowering the barriers between local minima the method effectively allows tunneling, promoting movement to another

minimum.

Other methods use a combination of procedures, such as random generation, movement and mutation of a solution to explore the surface, making decisions based on the fitness of a given solution to 'intelligently' explore a given search space and are termed meta-heuristics. Due to the random elements used in meta-hueristic algorithms many algorithms are often classified as either category.

A common meta-heuistic is Ant-colony optimization [77]. This mimics the action of ants looking for food, when an ant finds food it leaves a pheromone trail back to its nest. Other ants are more likely to follow the path, reinforcing it with more pheromone, than continuing to travel at random. Over time the pheromone trail evaporates, reducing its strength. The longer it takes an ant to travel the path the weaker it becomes. This means a short path will become more attractive, faster, than a longer one leading to an optimal soloution. Several other algorithms have been developed based on swarm intelligence such as Particle Swarm Optimization [78] and Bees optimization [79] (also known as Bee colony optimization).

4.2 The VCHAM Genetic Algorithm

The global optimization method selected for our purposes is the genetic algorithm. This a common meta-huerisitic which tries to mimic evolution and natural selection in order to reach the optimal solution. It is an iterative method where subsequent 'generations' of potential solutions are subjected to mutation operators, crossover operators and fitness based selection. In our case the fitness of a given solution is the root mean square of the standrad deviation (RMSD) between the model surface and the ab-initio reference points.

4.2.1 Intitial Population

The initial population, or initial parameter sets, is usually generated at random. The option exists, as used in other genetic algorithms, to seed the initial population with any number of user generated parameter sets. Early testing showed that placing user generated parameter sets in the initial population often led to early convergence on seeded paramter sets without any real exploration of the search space, although several other techniques are available, and discussed below, to avoid this early convergence making this a viable approach. Seeding the intitial population also has its uses as a means to further analyse previous results or as a way of continuing a previous optimization.

The initial parameters are scaled by the frequency of the relevent mode as shown in equations 4.6-4.10. By scaling to the frequency of the mode we can dramatically reduce the search space, which in turn reduces the time needed for the algorithm to converge.

$$\kappa_{i,s} = r\omega_i \tag{4.6}$$

$$\lambda_{i,s,s1} = r\omega_i \tag{4.7}$$

$$\gamma_{i,j,s,s1} = r\sqrt{\omega_i\omega_j} \tag{4.8}$$

$$\mu_{i,j,s,s1} = r\sqrt{\omega_i\omega_j} \tag{4.9}$$

$$\iota_{i,i,j,s,s1} = r\sqrt[3]{\omega_i\omega_i\omega_j} \tag{4.10}$$

4.2.2 Mutation Operator

The mutation operator is used to maintain diversity in the population and provide another means to leave a local minimum. This is often achieved by changing arbitrary values to a new value, this is decribed in equations 4.11,4.15 where greek characters denote coupling parameters, the superscript mut denotes the mutated value and ini denotes the initial value, r is a random number generated between -0.5 and 0.5, s is a scaling factor described below and ωi is the frequency of mode i.

$$\kappa_{i,s}^{mut} = \kappa^{ini} + (rs\omega_i) \tag{4.11}$$

$$\lambda_{i,s,s1}^{mut} = \lambda^{ini} + (rs\omega_i) \tag{4.12}$$

$$\gamma_{i,j,s,s1}^{mut} = \gamma^{ini} + (rs\sqrt{\omega_i\omega_j}) \tag{4.13}$$

$$\mu_{i,j,s,s1}^{mut} = \mu^{ini} + (rs\sqrt{\omega_i\omega_j}) \tag{4.14}$$

$$\iota_{i,i,j,s,s1}^{mut} = \iota^{ini} + (rs\sqrt[3]{\omega_i\omega_i\omega_j}) \tag{4.15}$$

The optional scaling factor, s, can be used to lower the magnitude of the mutation as the optimisation progresses. This factor was added after preliminary tests showed that large mutations late in the opimization caused such a significant increase in the deviation from the ab-initio reference points that all mutated parameter sets were dropped from the population within a few generations making the mutation operator ineffective as a source of new parameter values and as a means of maintaining diversity.

The danger with this scaling is that in the latter stages of the genetic optimization the mutations are so small that the new parameter sets generated

were within the same local minima as the initial parameter set. As another means of reducing this risk, while still limiting mutations, was to reduce the ratio of mutated parameters to those left at their initial value rather the magnitude of the parameter change. This is implemented as a probabilty, resulting in a greater variation of mutated parameter sets than a fixed ratio.

4.2.3 Crossover Operator

The crossover operator is used to vary the parameter sets from one generation to the next by generating new sets of parameters from a mixture of multiple 'parent' parameter sets. It is analogous to biological reproduction. This is eachieved by randomly pairing the population and producing two 'child' parameter sets from a mixture of the two parents' parameters. The first child is generated by taking each parameter from one of its parents at random, the second child is generated from the parameters not used by the first child. This crossover method is called 'uniform crossover'. In many genetic algorithm implementations this step is fitness based, so that only the best parameter sets go on to populate the next generation. In the VCHAM genetic algorithm it is only the selection operator that makes decisions based on fitness in order to minimise the number of times the deviation from the ab-initio reference points, as this is the most time consuming part of the algorithm (computational details are given in a the section below). This type of algorithm is termed 'elite selection' as it allows parent parameters sets to compete the child parameter sets.

4.2.4 Selection

The selection operator removes parameter sets based on their fitness, in this case a lower RMSD from the ab-initio reference points. This aims to preserve some of the weaker parameter sets in order to maintain genetic diversity. In the VCHAM genetic algorithm this is implemented using tournament selection. Tournament selection is where two parameter sets are selected at random and the set with the lower deviation from the ab-initio sets is put into the next generation. By only considering two at a time we preserve some weaker parameter sets.

4.2.5 Termination

The final operator, termination, halts the algorithm when any number of user specified end-conditions have been met. Typically this is a specified limit in order to avoid unneccessary computational expense, such as a maximum number of generations or a time limit. The algorithm will also terminate when the change in deviation from the ab-initio reference points from one interation to next reaches a suitable cutoff, typically $1 * 10^{-9}$ eV.

4.2.6 Local Populations

Initial testing showed that as the algorithm proceeds a tendency for sizeable proportions of the population has very similar values, decreasing the efficiency of the algorithm. To counter this tendency a new operator was added which compared each parameter set against the rest of the population and identify those with similar values. Once identified these 'local' populations are reduced in size to a fixed percentage of the population, typically five

percent.

Those that are removed are replaced with a new parameter sets generated at random using the same method as the initial population operator. This has the effect of greatly increasing the genetic diversity and the effeciency of the algorithm when these local populations arise. As the algorithm is quite expensive computationaly and ineffective before local populations arise this operator is only used after fifty generations as local populations tend not to arise early on.

4.3 Cyclobutadiene: A Test Case

4.3.1 Introduction

In order to test the genetic algorithm we required a suitable case, specifically one which has been studied before both experimentally and theoretically previously. Previous work undertaken by Saddique and Worth [12] into cyclobutadiene used a locally optimized VCHAM and also calculated a photo-electron spectrum that was compared with experimental work on the same molecule. The model used had 18 degrees of freedom, 3 electronic states and 128 non-zero parameters (using a second order model). Despite cyclobutadiene's simplicity the previous calculation was not able to accurately reproduce the photo-electron electron spectrum quantitatively.

Over the last century [80] cyclobutadiene and it's derivatives have been studied extensively, and for much of this time several of its fundamental properties were under dispute. One might expect initially the cyclobutadiene would have a square planar ground state geometry. However the Huckel $4n+2$ rule predicts this to be unstable, as experiment [13] and calculations [18, 81, 82]

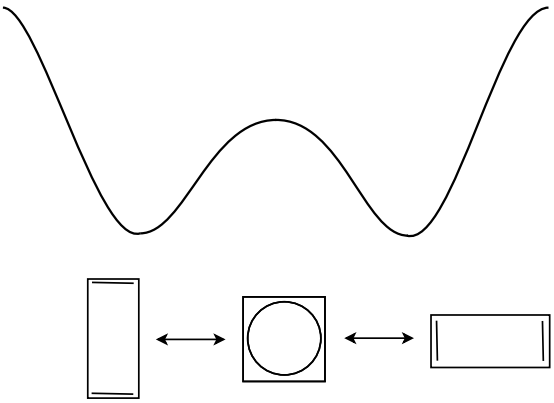

Fig. 4.1: Potential energy surface along a hypothetical reaction co-ordinate linking the two rectagular forms of cyclobutadiene.

showed. This can be explained by vibronic coupling between the $\widetilde{X}^1B_{1g}$ and the A^1A_{1g} state at D_{4h} which induces the lowering of symmetry and results in a rectangular structure with lower symmetry (D_{2h}), as apposed to a square ground state with D_{4h} as illustrated in figure 4.1. This is also referred to as a second-order or pseudo Jahn-Teller as the two states are not electroncally degenerate despite the orbital degeneracy (see figure 4.2).

Cyclobutadiene has been of interest theoretically for some time [80] and has been frequently used to help explain quite challenging experimental work [83, 84]. Early experimental work on cyclobutadiene was often hampered by the difficulty in synthesis, which often led to by products (notably CO_2 [85]) which interfered with analysis. This in itself led to significant efforts studying derivatives of cyclobutadiene, hoping to block dimerisation without significantly perturbing the π system. It was not until it was possible to photochemically generate cyclobutadiene in a noble gas matrix at cryogenic temperatures that the parent compound could be studied directly [13, 14, 86, 87].

While virtually all theoretical calculations agreed qualitatively that cyclobutadiene in its S_0 state would have a rectangular equilibrium geometry the

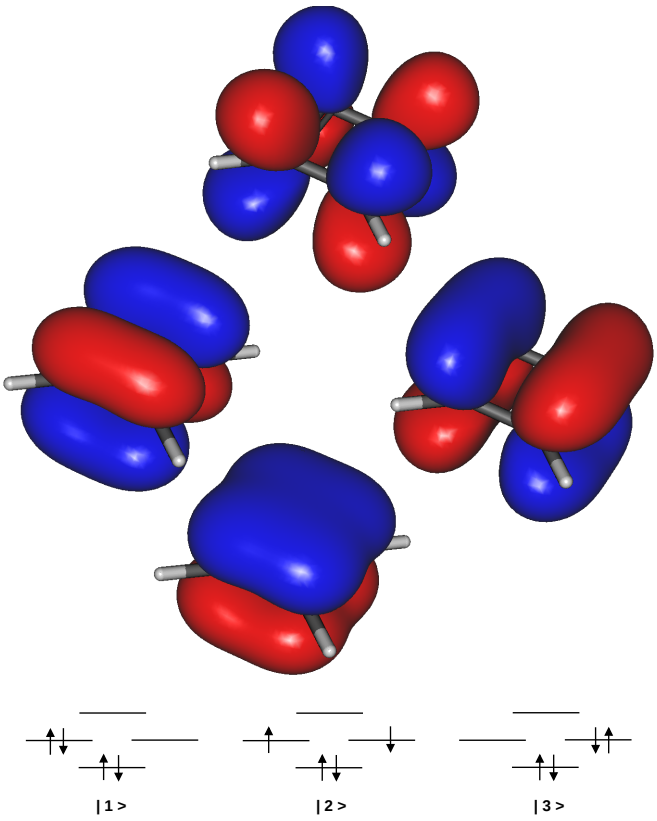

Fig. 4.2: The four molecular orbitals, ϕ_1-ϕ_4 of cyclobutadiene defining the active space and the three configuration $|1>$, $|2>$ and $|3>$ which describe the lowest three singlet states

relative energies of the lowest singlet state at D_{4h} geometry were often in disagreement. Of particular importance were Allingers PPP-CI calculations [88,89] which showed that the D_{2h} geometries would have no transitions above 200nm, where as the D_{4h} would have a significant transition at approximately 370nm which was later used to help analyse the experimental work.

4.3.2 Previous Application of the VCHAM

As mentioned above, the previous theoretical work undertaken by Saddique and Worth used local optimization to fit the VCHAM to the ab-initio reference points. This fitted VCHAM was then used in a wave packet propogation calculation in order to calculate the photo-electron spectrum, and compare to experimental work. The experimental photo-electron spectrum, taken by Kohn and Chen [13] and shown in figure 4.3 is the spectrum with highest vibrational resolution to date. The previous work was able to qualitatively reproduce the experimental spectrum (see figure 4.4) but unable to reproduce the vibrational progression quantitatively. In the work by Saddique and Worth [12] a six mode second order spectrum was also calculated, which is reproduced in figure 4.5. Although the vibrational progression is the same in both spectra, the larger model was unable to match the experimental features as closely.

In their own paper Kohn and Chen produced a model spectrum (Figure 4.6) alongside the experimental which was also unable to quantitatively reproduce the vibrational progression found in their experimental mode. As their model only included the vibrational modes which produce a rectangular distortion (b_{1g}) rhomboidal distortion (b_{2g}) and only using linear vibronic coupling it is quite limited in its scope and a model that includes additional

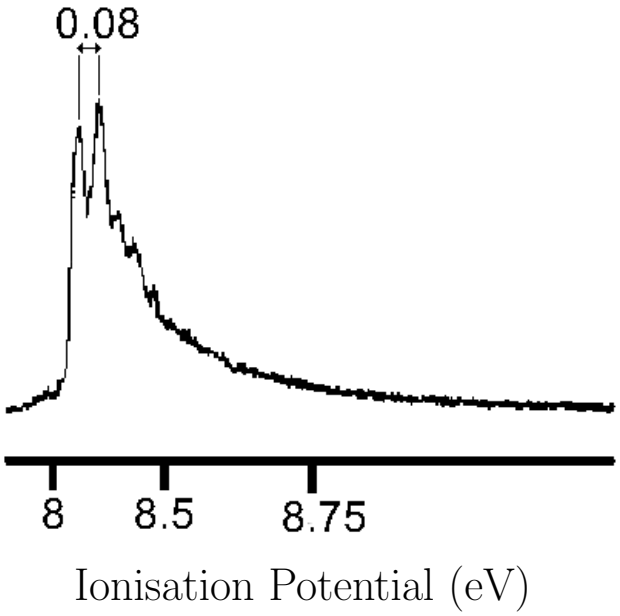

Fig. 4.3: Experimental photoelectron spectrum reproduced from [13], with a reported vibrational progression of 0.08 ± 0.03 eV of cylcobutadiene

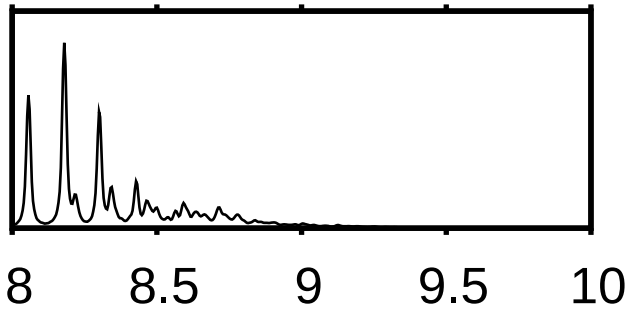

Fig. 4.4: Saddique and Worth spectrum reproduced from [12] with a vibrational progression of 0.18eV using a two mode linear model.

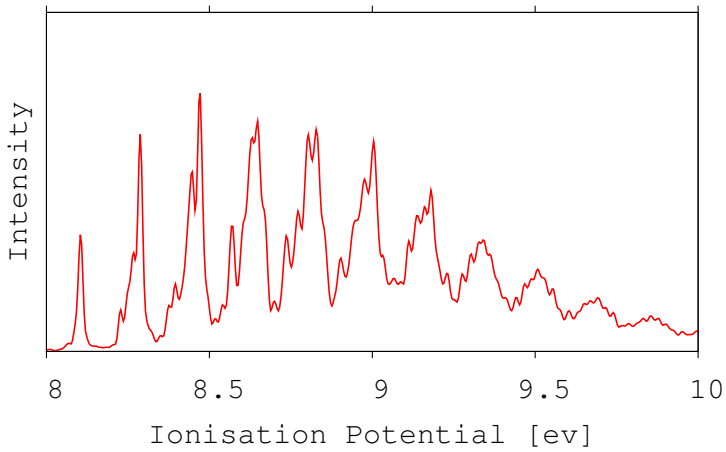

Fig. 4.5: Saddique and Worth spectrum reproduced from [12] with a vibrational progression of 0.18eV using a six mode second order model.

degrees of freedom, particularly those that break the D_{4h} symmetry of the square cyclobutadiene structure, as well as higher order terms in order to better describe the potential energy surface should be able to reproduce the experimental spectrum to a higher degree of accuracy.

Comparing the photo-electron spectrum is a more accurate method to determine whether the fitting procedure arrives at the correct coupling parameters in our model hamiltonian, as opposed to the best fit of the parameters to the ab-initio reference points. With the computational expense of a full space search, this provides us with an excellent way of determining whether our parameters are accurate.

4.3.3 Applying the Genetic Algorithm

In order to compare the effectiveness of the genetic algorithm the potential energy surface was calculated along every vibrational mode and between all of those where symmetry allowed coupling. To set up the model the

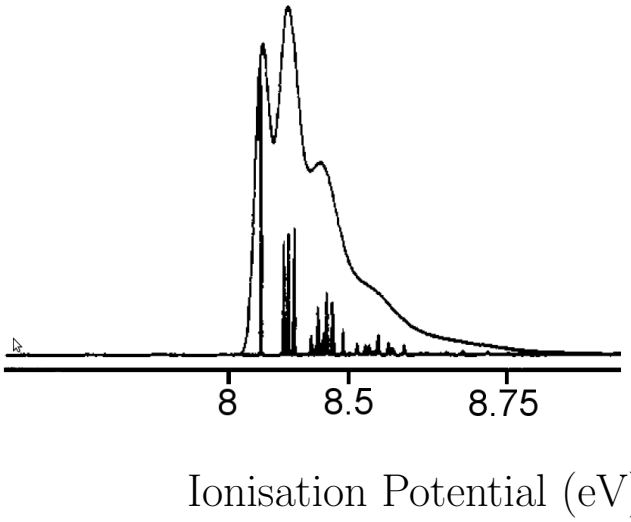

Fig. 4.6: Model photoelectron spectrum reproduced from [13], with a vibrational progression of 0.29 eV (The scale and quality of the spectra make this difficult to determine accurately)

geometry was optimised using CASSCF and a 6-31g* basis set using the GAUSSIAN [90] quantum chemistry package, as was performed in the previous theoretical work by our group. Defining the symmetry with the C_2 axis bisecting the bonds and C_2' bisecting the atom (Same as in the review by Nakamure et. al. [18]) we expanded about the equilibrium geometry here after referred to as Q_0.

Using frequencies calculated at the CASSCF level (Table 4.1) geometries were calculated along each vibration, and between vibrations where coupling is allowed by symmetry, and their energies calculated at the CASPT2 level using the 6-31g* basis set and the MOLPRO [91] quantum chemistry package. The same active space was used as in the previous work, namely the four π moleculate orbitals ϕ_1-ϕ_4 shown in 4.2. CASPT2 is a signicant improvement over the previous work where the CASSCF method was used, but as it was cited that inaccuracies in the potential energy surface were the reason for the difficulty in quantitatively reproducing the photo-electron spectrum it seemed prudent to use a method that accounted for electron correlation.

Mode	MP2	CAS(4,4)	Experimental
$1a_u$	471.9	535.1	-
$1b_{2g}$	490.0	432.4	531
$1b_{2u}$	554.0	524.1	576
$2a_u$	710.0	734.4	-
$1b_{2u}$	749.8	852.6	721
$1b_{1g}$	777.3	699.6	-
$1b_{3g}$	858.7	966.3	723
$1a_g$	991.6	999.3	989
$1b_{1u}$	1080	1131	1028
$2a_g$	1149	1215	1059
$2b_{3g}$	1201	1307	-
$2b_{2u}$	1292	1411	1245
$3a_g$	1601	1513	1678
$2b_{1u}$	1615	1640	1526
$3b_{3g}$	3264	3403	3093
$3b_{2u}$	3278	3417	3107
$3b_{1u}$	3298	3430	3124
$4a_g$	3307	3445	3140

Table 4.1: Frequencies of neutral cyclobutadiene calculated at the D_{2h} minimum energy geometry using both MP2 and CASSCF methods (using a 6-31G* basis set) compared to experimental frequncies in cm^{-1}. Experimental frequencies are taken from reference [14] except for $1b_{1u}$ which is taken from refence [15].

These calculations gave us a database of 483 reference points (the odd number is due to the failure of some calculations to converge). This provides a more than adequate description of the potential energy surface. The number of points used is higher than required in order that the test accurately reflects the black box nature of the genetic algorithm. The number of reference points could be greatly reduced, particularly for harmonic modes where no loss of features would occur. Often this is done in order to avoid computational expense, as in order to evalute the RMSD the model needs to be calculated for each reference point.

For a second-order on-diagonal model this gives 482 parameters. This model is used for comparison with the previous theoretical work by our group, a full model is discussed in section 4.3.4. Using a small population of 100 and

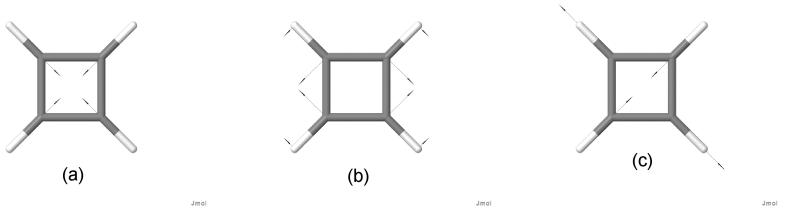

Fig. 4.7: The vibrational modes (a) $\nu_1(1a_{1g})$ a ring stretching vibration, (b) $\nu_4(2b_{1g})$ a rectagular vibration and (c) $\nu_6(1b_{2g})$ a romboidal vibration.

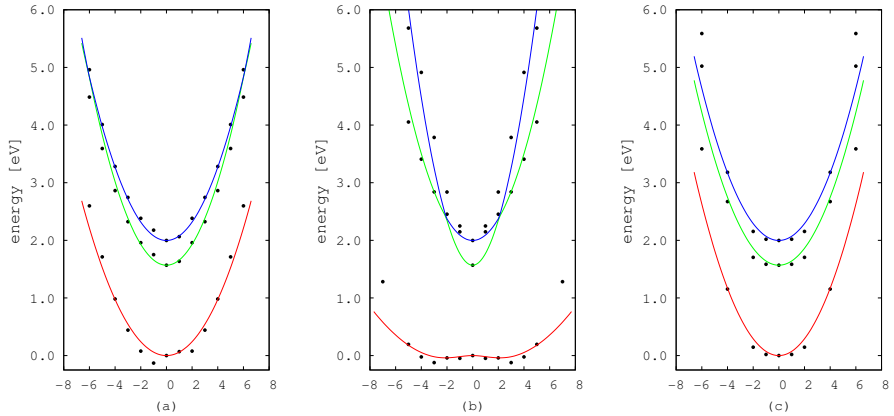

Fig. 4.8: Calculated ab-initio points (using CASPT2) and fitted surfaces from the Genetic Algorithm along the vibrational modes (a) $\nu_1(1a_{1g})$, (b) $\nu_4(2b_{1g})$ and (c) $\nu_6(1b_{2g})$ using an on-diagonal second order model.

terminating the algorithm after 200 generations an acceptable fit was calculated. This calculation took only 20 minutes on a standard linux workstation (2.4Ghz Pentium 4 with 512MB of RAM). Example vibrational modes modes from these fits are shown in figure 4.8 and figures depicting the vibartional modes are shown in figure 4.7. Further optimization using the conjugate gradient method gives considerably better fits 4.9, lowering the root mean square of the deviation (RMSD) of the model to the ab-initio reference points from 11.3 to 0.18 eV. This is still higher than in the previous theoretical work, which has a RMSD of 0.069 eV, which can be ascribed to the increased number of modes in the system with anharmonicity which cannot be adequately described by the harmonic oscilator used as the zeroth order potential. In

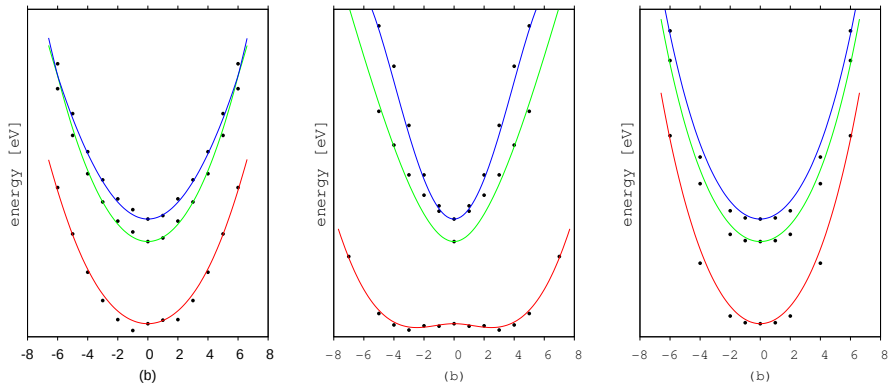

Fig. 4.9: Calculated ab-initio points (using CASPT2) and fitted surfaces from the Genetic Algorithm and Conjugate Gradient algorithm along the vibrational modes (a) $\nu_1(1a_{1g})$, (b) $\nu_4(2b_{1g})$ and (c) $\nu_6(1b_{2g})$ using an on-diagonal second order model.

the more complete model described in theory chapter this is overcome by using morse potentials as the zeroth order potential. The photo-electron spectrum (Figure 4.10) was calculated using wavepacket dynamics simultions performed using the MCTDH method. The first step was to obtain the ground state nucleur wavefunction for the neutral molecule by propagating in imaginary time to a guess wavepacket using the vibronic coupling model Hamiltonian neutral molecule. The guess wavepacket was then taken as the ground state harmonic oscillator eigenfunction of the zero-order hamiltonian. The nuclear wavefunction at time t, $\Psi(t)$, is then obtained by solving the time-dependent Schrödinger equation, allowing the initial wavefuntion to evolve over the set of surfaces. The spectrum calculated in this manner is shown in figure 4.10 which, is able to reproduce the appearence of the experimental spectra qualitatively as well as yielding a vibrational progression of 0.12 eV, signifcantly closer to the experimental value of 0.08 $\pm$ 0.03 eV than the previous work by Saddique and Worth.

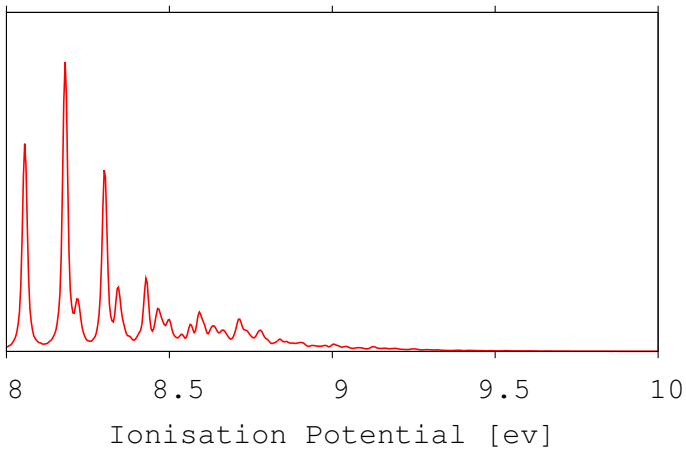

Fig. 4.10: Theoretical spectrum produced using parameters from the combined genetic algorithm and conjugate gradient approach using an on-diagonal second order model, with a vibrational progression of 0.12eV.

4.3.4 18 mode Cyclobutadiene model

Using the same database of ab-initio reference points a 3rd order model (fitting out to off diagonal quadratic-linear co-ordinate ι) was fitted using the genetic algorithm. This required the fitting of 1211 non-zero parameters and as mentioned above for the anharmonic modes morse potentials were used. This calculation took 56 minutes, compared to the previous calculation which required only 20 minutes. Example modes from the genetic algorithm fit are shown in figure 4.11 as are the fits after subsequent local optimization using the conjugate gradient method in figure 4.12. As you can be seen from figure 4.11 the genetic algorithm is quite capable of fitting parameters for these surface. However upon local optimisation (Figure 4.12) some of the work is undone as the local optimiser rejects the upturned nature of S_1 along the $\nu_9(1B_{3g})$ normal mode. By using morse functions it was possible to produce a better fit to the ab-initio surface for $\nu_1(1a_{1g})$. Using the VCHAM fitted with the combined genetic algorithm local optimisation approach and now all 18

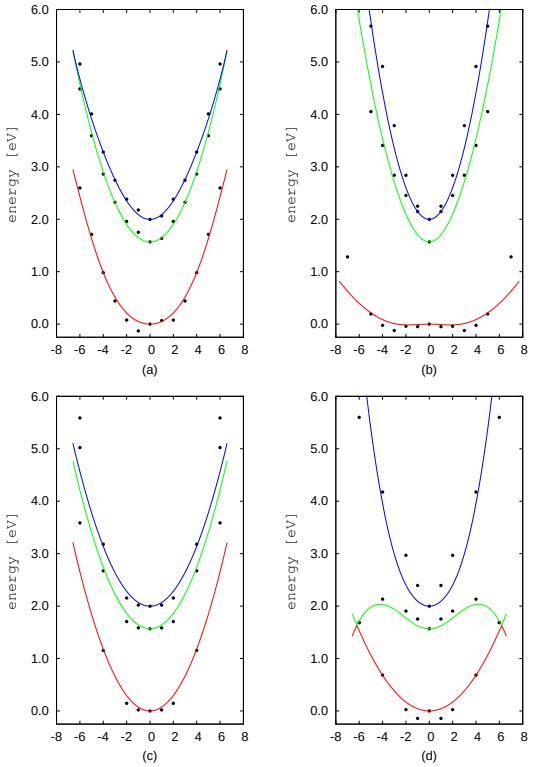

Fig. 4.11: Calculated ab-initio points and fitted surfaces from the Genetic Algorithm along the vibrational modes (a) $\nu_1(1a_{1g})$, (b) $\nu_4(2b_{1g})$, (c) $\nu_6(1b_{2g})$ and (d) $\nu_9(1b_{3g})$ using an off-diagonal third order model.

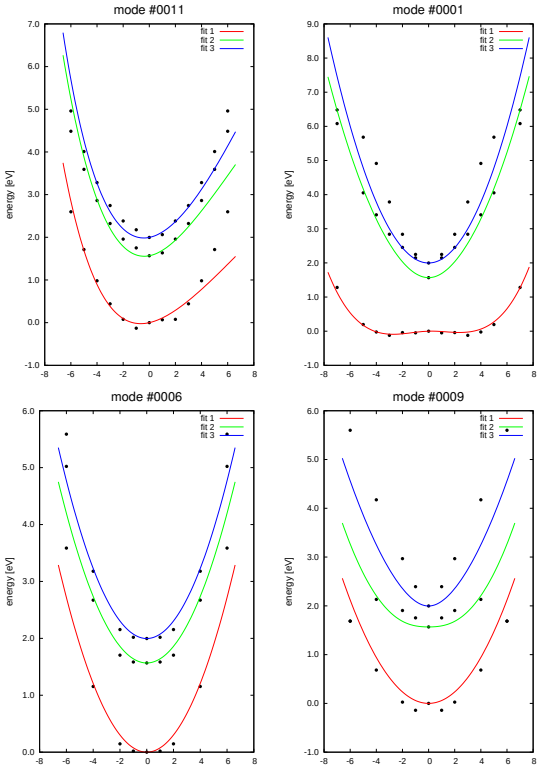

Fig. 4.12: Calculated ab-initio points and fitted surfaces from the Genetic Algorithm and Conjugate-Gradient optimization along the vibrational modes (a) $\nu_1(1a_{1g})$, (b) $\nu_4(2b_{1g})$, (c) $\nu_6(1b_{2g})$ and (d) $\nu_9(1B_{3g})$ using an off-diagonal third order model.

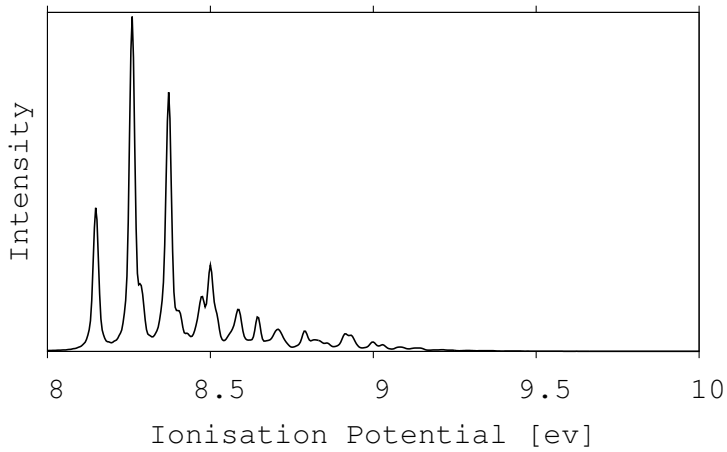

Fig. 4.13: Theoretical spectrum produced using parameters from the combined genetic algorithm and conjugate gradient approach using an off-diagonal third order model, with a vibrational progression of 0.12 eV

modes, as opposed to the previous spectrum which used the same vibrational modes as the original spectrum calculated by Saddique and Worth [12]. The spectrum, shown in figure 4.13, has the same vibrational progression (0.12 eV) as the 6 mode genetical algorithm shown above (Figure 4.10) as well as fitting the general shape shown in the experimental spectrum (Figure 4.3). Without an experimental spectrum of higher resolution it is difficult to say whether the 18 mode model has improved over the 6 mode model.

Chapter 5

Allene and Pentatetraene

As a further test for the genetic algorithm two molecules previously studied using the MCTDH method were selected and a new VCHAM fitted to the previously calculated PES. By using the same PES surface as that used by the previous study, differences in the calculated absorption spectrum would be due to differences in fitting procedure. Both allene [10] and pentatetrane [10, 11] display strong coupling effects involving cationic states with degenerate components. These can be represented as localised charge at either end of the allene and pentatetrane molecules.

5.1 Allene

5.1.1 Introduction

The original work using MCTDH on allene [10] was undertaken in order to simulate the charge transfer process. This was achieved by artificially depopulating one component and observing the transfer of charge into the depopulated component.

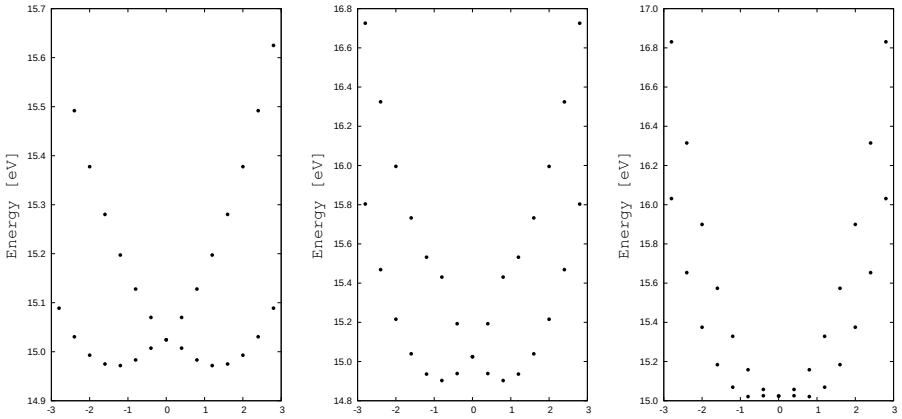

Fig. 5.1: A diagram showing cuts through the potential energy surface along modes $\upsilon 4(B_1)$,$\upsilon 5(B_2)$ and $\upsilon 8(E)$ (from left to right).

5.1.2 Potential Energy Surface

The intial geometry optimisation and vibrational normal mode calculations were taken from the previous work [10], where they were calculated using the MP4 method and a the 6-311G* basis set. This was used to generate geometries with which to build up the PES. Unlike previously where normal mode co-ordinates were used, the allene work used rectilinear normal coordinates. The excited states were then calculated using the ab-initio outer-valence green's function (OVGF) [92,93] method along the non-degenerate modes. as implemented in the GAUSSIAN 98 program [94]. The OVGF method ionises a single valence electron from its HF orbital and determines the ionisation energy using a Green's function aproach. The degenerate modes, due to failures in the OVGF method, were calculated using th ADC(3) method [95]. Some example cuts can be seen in figure 5.1.

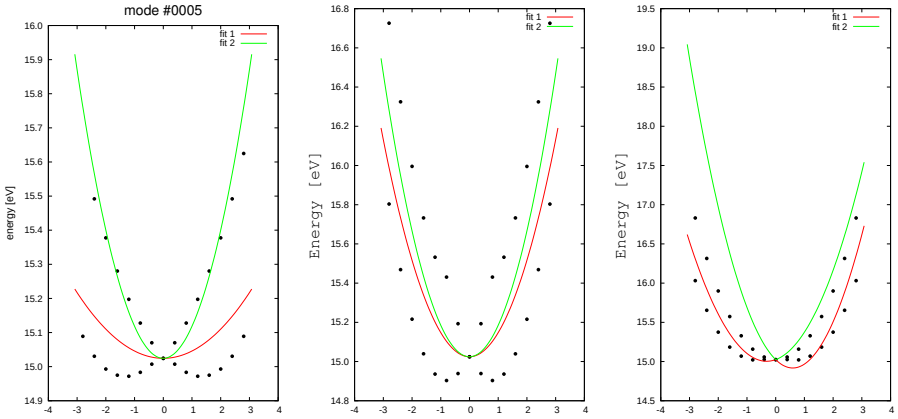

Fig. 5.2: A diagram showing genetic algorithm fits of the VCHAM along the modes $\upsilon 4(B_1)$,$\upsilon 5(B_2)$ and $\upsilon 8(E)$ (from left to right)

5.1.3 Model Hamiltonian

Using the calculated PES from the previous work by Markman et. al. [10] a genetic algorithm optimisation was performed with a population of two thousand for three hundred generations. The VCHAM was used up to second order off-diagonal terms with 176 non-zero coupling terms to be optimised. Some example modes with the VCHAM fits overlaid are shown in figure 5.1. As can be see from figure 5.1 the genetic algorithm frequently performed rather poorly when dealing with very large coupling terms (those modes with very deep wells.) When optimising locally the lower energy points are often given a greater weighting than the higher energy points to ensure the well height is accurate. The genetic algorithm was run without this energy weighting in order to test its robustness, but it appears energyweighting may be neccessary in further genetic algorithm runs.

Using the genetic algorithm as an initial guess for local optimisation, where large energy-weighting was used, the VCHAM parameters were further fitted. Some example fits of the final VCHAM are shown in figure 5.3.

In order to compare the parameters from both fits those parameters cal-

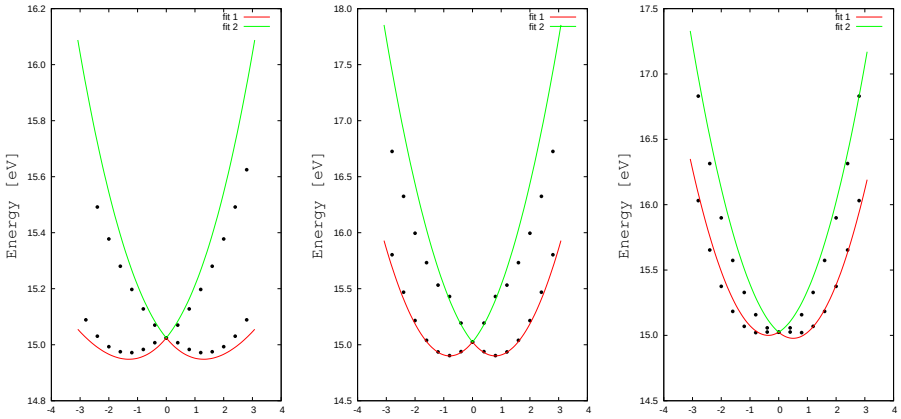

Fig. 5.3: A diagram showing combined genetic algoirthm and local optimisation fits of the VCHAM along the modes $\upsilon 4(B_1)$,$\upsilon 5(B_2)$ and $\upsilon 8(E)$ (from left to right)

i	Symmetry	$\kappa_i^{(1)}$	$\kappa_i^{(3)}$	$\kappa_i^{(4)}$	$\gamma_{ii}^{(1)}$	$\gamma_{ii}^{(3)}$	$\gamma_{ii}^{(4)}$	$\gamma_{ii}^{(5)}$
1	A_1	-0.3767	-0.6400	-0.4327	-0.0562	-0.0248	0.0207	-0.0140
2	A_1	-0.2482	0.3926	0.3472	0.0000	-0.0295	-0.0359	-0.0264
3	A_1	-0.1993	-0.2089	0.1573	-0.0348	-0.0248	-0.0215	-0.0104
4	B_1				-0.0689	0.0762	-0.0781	-0.0008
5	B_2	0.4132			0.0000	0.0000	0.0000	0.0000
6	B_2	0.1003			-0.0156	-0.1641	-0.0201	0.0310
7	B_2	0.3200			-0.2460	0.0000	0.0000	0.0000
8	E				-0.0361	-0.1001	0.1592	0.0104
9	E				-0.0363	-0.0361	-0.0173	-0.0013
10	E				0.0000	-0.0115	-0.0113	-0.0109
11	E				-0.0247	-0.0222	-0.0903	-0.1410 s

Table 5.1: Linear and quadratic coupling parameters (in eV) for Allene calculated used a combined genetic alogoirthm local optimisation approach.

culated with the combined genetic algorithm local optimisation method discussed above are presented along with those calculated using only local optimisation in the original work on allene [10]. The first table 5.1 shows the linear and quadratic on-diagonal coupling paramaters from this work and the second table 5.2 shows the same parameters taken from Table II in [10].

i	Symmetry	$\kappa_i^{(1)}$	$\kappa_i^{(3)}$	$\kappa_i^{(4)}$	$\gamma_{ii}^{(1)}$	$\gamma_{ii}^{(3)}$	$\gamma_{ii}^{(4)}$	$\gamma_{ii}^{(5)}$
1	A_1	-0.4471	-0.2762	-0.4491	-0.0251	-0.0029	0.0166	
2	A_1	-0.2527	0.4702	0.3564	-0.0492	-0.0311	-0.0265	
3	A_1	-0.1874	-0.0237	0.0988	0.0000	0.0000	-0.0117	
4	B_1				-0.0418	-0.1656	-0.0788	
5	B_2	0.3364			0.0440	0.0036	-0.0020	
6	B_2	0.0865			0.0073	0.0037	-0.0206	
7	B_2	0.3163			-0.0530	-0.0688	0.0020	
8	E				0.0061	-0.0813	0.1674	
9	E				-0.0164	-0.0434	-0.0152	
10	E				0.0216	-0.1656	-0.0112	
11	E				-0.0200	-0.0600	-0.0828	-0.1320

Table 5.2: Linear and quadratic coupling parameters (in eV) for Allene using local optimisation taken from [10]

5.1.4 Absorption Spectrum

Using the VCHAM fitted using the combined genetic algoithm local optimisation approach an absorption spectrum was calculated 5.5 and compared to the experimental spectrum in figure 5.4 reproduced from reference [96].

5.2 Pentatetraene

5.2.1 Introduction

Pentatetraene was previously studied using a VCHAM [10] and used to generate a simulated photoelectron spectrum of the pentatetraene cation [11].

5.2.2 Potential Energy Surface

As with qllene the intial geometry optimisation and vibrational normal mode calculations were taken from the previous work [10], where they were calculated using the MP4 method using the 6-311G* basis set. This was used to generate geometries with which to build up the PES. Unlike previously

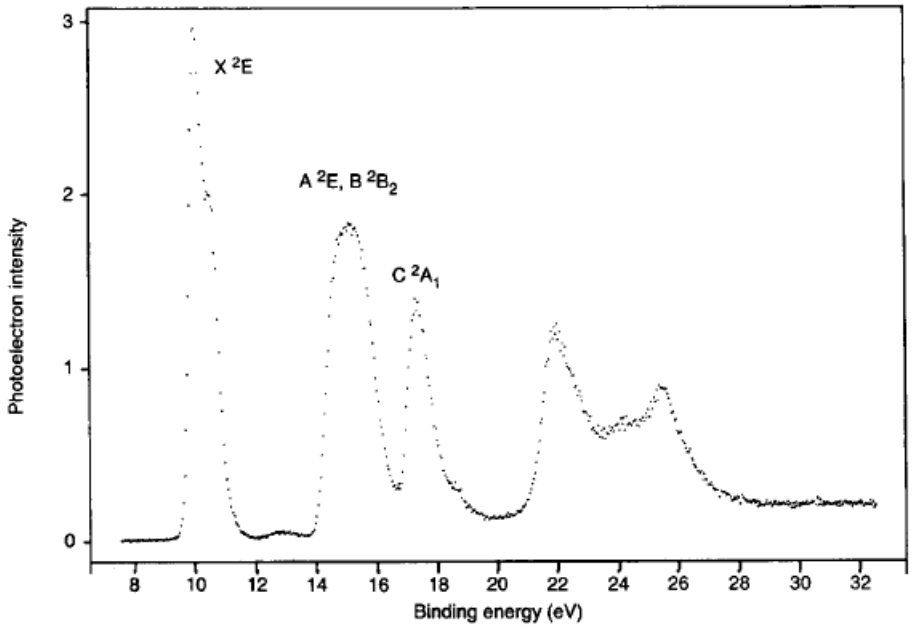

Fig. 5.4: The absorption spectrum of allene taken from reference [96]

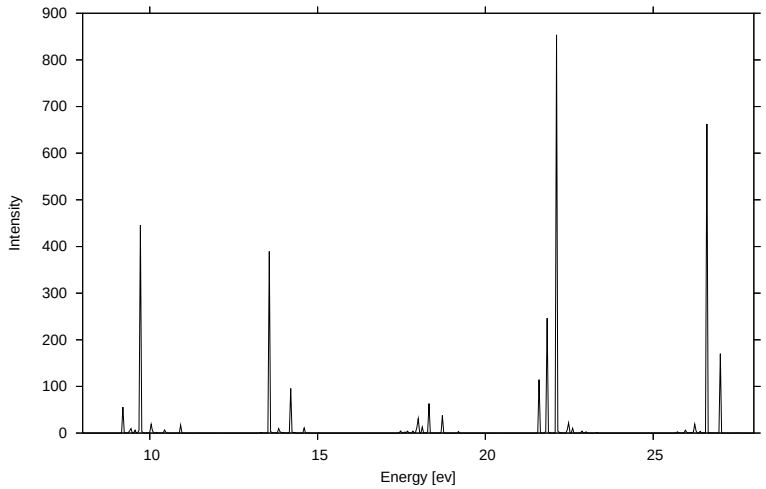

Fig. 5.5: The absorption spectra of allene calculated using the VCHAM fitted using the combined genetic algorithm local optimisation approach.

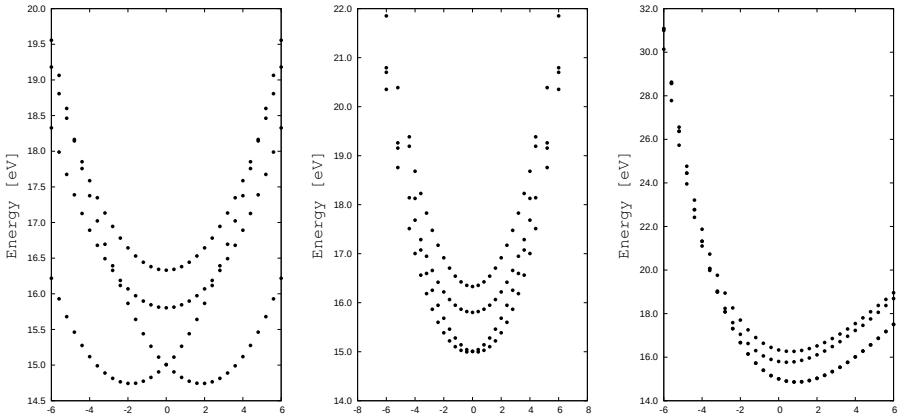

Fig. 5.6: A diagram showing cuts through the potential energy surface along modes $\upsilon 13(B_2)$,$\upsilon 17(B_2)$ and $\upsilon 19(A_1)$ (from left to right)

where normal mode co-ordinates were used, the allene work used rectilinear normal coordinates.

The excited states were then calculated using the ab-initio outer-valence green's function (OVGF) [92, 93] method along the non-degenerate modes. as implemented in the GAUSSIAN 98 program [94]. The OVGF method ionisaes a single valence electron from its HF orbital and determines the ionisation energy using a Green's function aproach. The degenerate modes, due to failures in the OVGF method, were calculated using th ADC(3) method [95]. Some example cuts can be seen in figure 5.6.

5.2.3 Model Hamiltonian

Using the calculated PES from the previous work by Markman et. al. [10, 11] a genetic algorithm optimisation was performed with a population of two thousand for two thousand generations. Some example modes with the VCHAM fits overlaid are shown in figure 5.7. Again the Genetic Algorithm is unable to fit deep wells ($\upsilon 13(B_2)$) and anharmonic surfaces ($\upsilon 19(A_1)$).

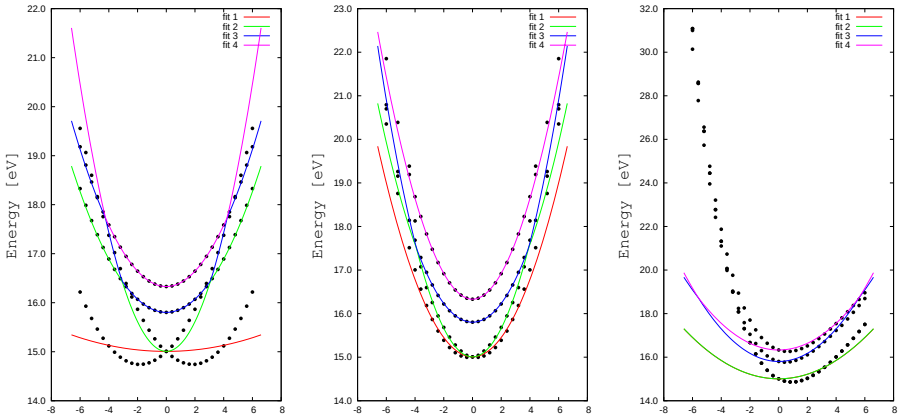

Fig. 5.7: A diagram showing genetic algorithm fits of the VCHAM along modes $\upsilon 13(B_2)$,$\upsilon 17(B_2)$ and $\upsilon 19(A_1)$ (from left to right)

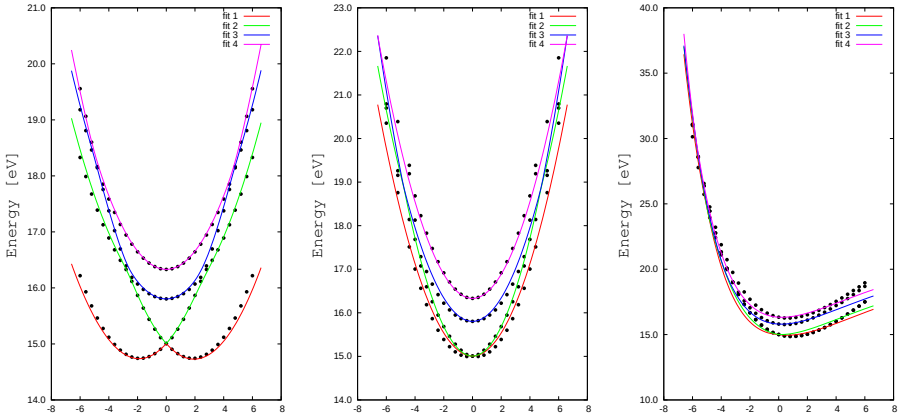

Fig. 5.8: A diagram showing combined genetic algoirthm and local optimisation fits of the VCHAM along modes $\upsilon 13(B_2)$,$\upsilon 17(B_2)$ and $\upsilon 19(A_1)$ (from left to right)

By adding Morse potentials as the zeroth order potential and applying an energy weighting on those modes with particuarly deep wells during local optimisation, better fits can be achieved. These combined genetic algorithm local optimisation fits are shown in figure 5.8.

5.2.4 Photoelectron Spectrum

Using the VCHAM fitted using the combined genetic algoithm local optimisation approach an absorption spectra was calculated (Figure 5.9) and

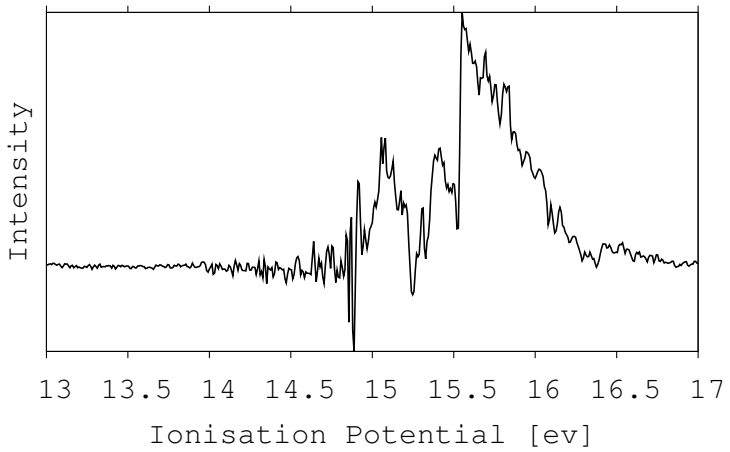

Fig. 5.9: The photoelectron spectrum of pentatetraene calculated using the VCHAM fitted using the combined genetic algorithm local optimisation approach.

compared to the experimental spectrum in figure 5.10 reproduced from reference [97].

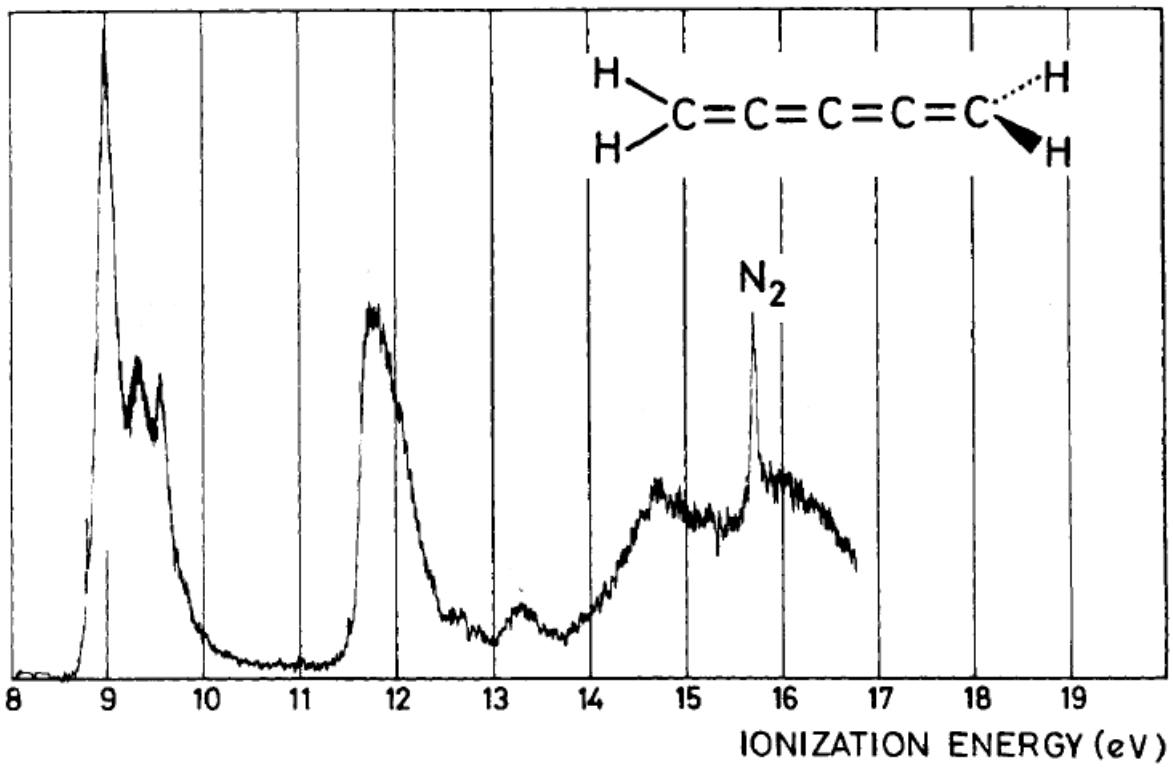

Fig. 5.10: The photoelectron spectrum of pentatetraene reproduced from [97].

Chapter 6

Toluene

6.1 Introduction

Toluene as a mono-substituted benzene derivative allows us to study the effect of the addition of a simple methyl group to benzene. As benzene derivates form a basis for a wide variety of organic compounds found in nature we can use toluene as a model for the effect of a simple rotation, from the methyl group, on the photophysics of similar compounds. Unlike benzene which has been studied in great detail both experimentally [98–101] and theoreticaly [102–105] the photophysics of toluene has been left largely unexplored since pioneering work in 1946 by Ginsburg et. al [106]. With initial work focusing on other derivates of benzene such as para-difluorobenzene and fluorotoluene [107–109], toluene was later explored in 1986 by Parmenter and Stone [110] with a view to exploring the effect of the methyl rotor as an IVR accelerator. They found that the iteraction of this degree of freedom with the vibrational modes induced rapid IVR.

In more recent work using time-resolved photo-electron velocity map imaging the Reid group have been able to explore this in much greater detail [111–113]. Particular attention is paid to the Fermi resonance at 457

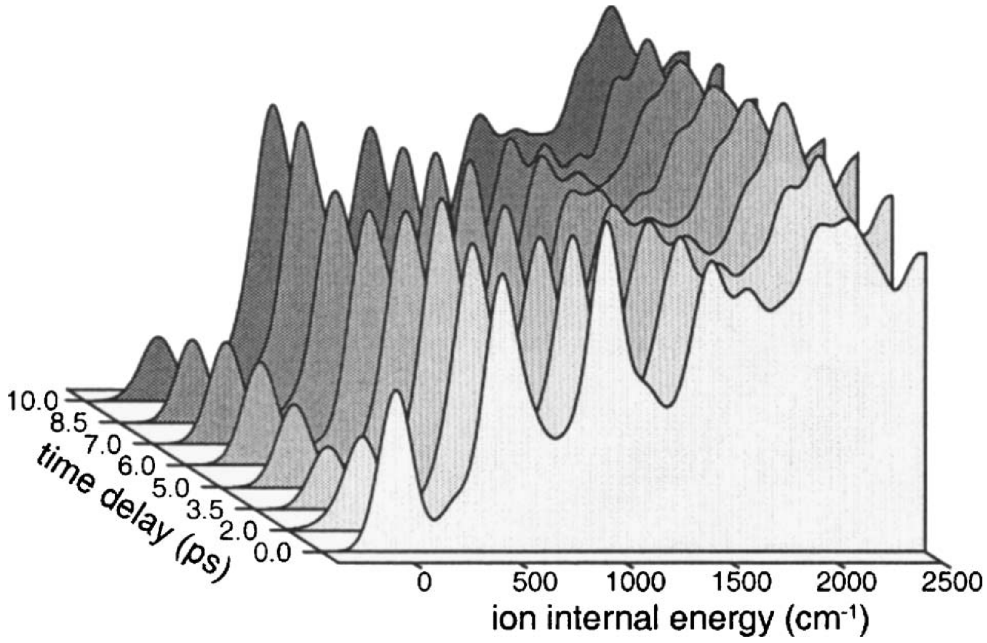

Fig. 6.1: Time Dependent Photoelecton Spectrum following the preparation of the $6a^1 + 10b^1 16b^1$ Fermi resonance at 457 cm^{-1} with a 1ps laser pulse, as a function of the time delay between excitation and ionization with a second identical laser pulse. Reproduced from [113]

cm^{-1} showing oscillations in the intensities of the $6a^1$ and $10b^1 16b^1$ peaks (shown in figure 6.1). In their most recent work [114] anharmonic coupling matrix elements were derived from their spectra.

In order to explore the photophysics of toluene a model Hamiltonian must be prepared in order to run wavepacket dynamics. To calculate points along the normal modes of toluene a frequency calculation is first performed. This was done by first optimising the geometry of toluene to its equilibrium geometry, with an experimentally determined equilibirum geometry as an initial starting point. This, and the subsequent frequency calculation, were performed at the MP2 level with a 6-31g* basis set. A comparison of calculated and experimentally determined frequencies is shown in figure 6.1.

Mode	Varsonyl Notation	MP2	Experimental	Descrition
2	$\upsilon 10_b$	207.29	216	CH_3 wag
5	$\upsilon 16_b$	451.58	464	para CH out of plane
6	$\upsilon 6_a$	502.98	521	Ring breathing
7	$\upsilon 6_b$	528.79	623	Ring bend
10	$\upsilon 18_a$	809.97	1030	Ring bend
14	$\upsilon 17_b$	887.64	3	CH out of plane
15	$\upsilon 9_a$	1024.36	3	CH rock
18	$\upsilon 12$	1148.24	1003	$C - CH_3$ stretch
22	$\upsilon 13$	1264.39	3	$C - CH_3$ stretch

Table 6.1: Comparison of calculated and experimental vibrational frequencies for selected vibrational modes of toluene. Experimental frequencies taken from [115]

This shows reasonably small differences between the calculated frequencies and the experimentally determined frequencies. With this information a number of geometries about the equilibrium geometry can be calculated along and between the vibrational modes in order to fit the VCHAM.

6.2 Potential Energy Surface

Points along the normal modes were initialy calculated using the CASSCF method and a 6-31g* basis set. The active space selected was that of the 3 bonding and 3 antibonding configurations of the out of plane p orbitals, as shown in figure 6.2. Some example cuts along the vibrational modes $\upsilon 10_b$, $\upsilon 16_b$ and $\upsilon 6_a$ (those that are involved in the Fermi resonance) are shown in figure 6.3.

To assess the accuracy of these calculations they were repeated at a higher level of theory, specifically the CASPT2 method using a slightly larger basis

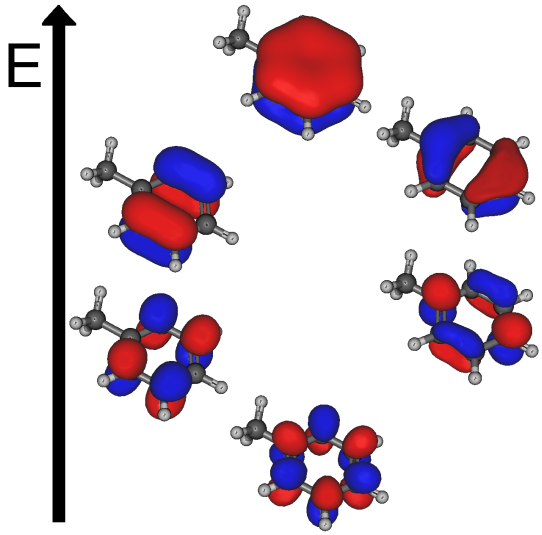

Fig. 6.2: A diagram showing the 6 molecular orbitals selected for the active space on toluene.

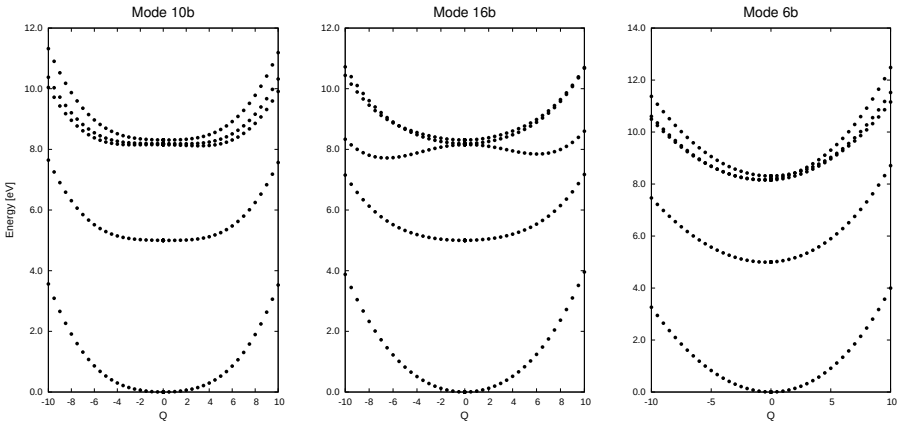

Fig. 6.3: Example cuts through the potential energy surface of toluene calculated at the CASSCF(6,6) level using a 6-31g* basis set. The cuts are along the vibrational modes $\upsilon 10_b$, $\upsilon 16_b$ and $\upsilon 6_a$ (left to right)

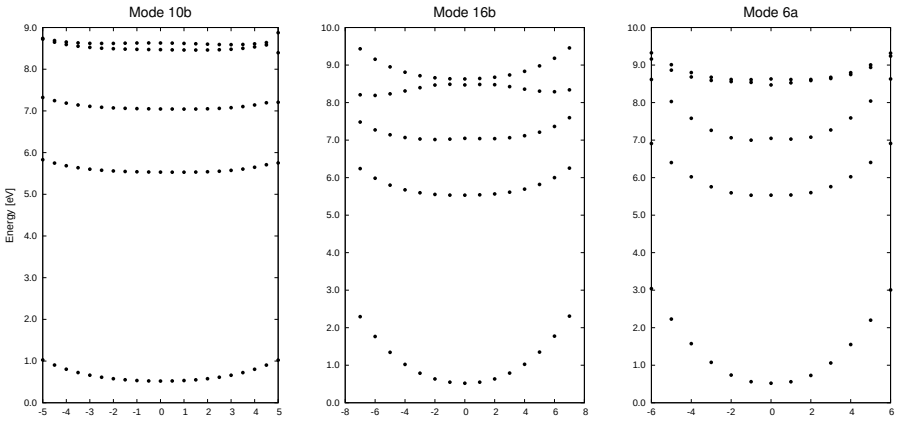

Fig. 6.4: Example cuts through the potential energy surface of toluene calculated at the CASPT2(6,6) level using a 6-31g** basis set. The cuts are along the vibrational modes $\upsilon 10_b$, $\upsilon 16_b$ and $\upsilon 6_a$ (left to right).

set (6-31g**) but the same active space. While superficially the results were similar, the energetics were quite different. Some example cuts along the same vibrational modes are shown in figure 6.4.

A more detailed comparison shows that rather than a small change in energy for the excited states the addition of electron correlation the CASPT2 calculations shifts the S_4 state in the CASSCF calculations to a lower energy than S_3, a change of 1.79 eV. A labelled comparison of the two calculations is shown in figure 6.5.

This also has the effect of changing the curvature of the S_2-S_4 surfaces, which would have a significant effect on the parameters fitted to these surfaces. It was also found that along some of vibrations the (6,6) active space was insufficient. Initially it was considered that increasing the active space to include the out of plane p orbitals on the methyl group (orbitals on the right in figure 6.6) would increase the stability. Calculations however showed that this was not the root of the problem and that the geometries that were

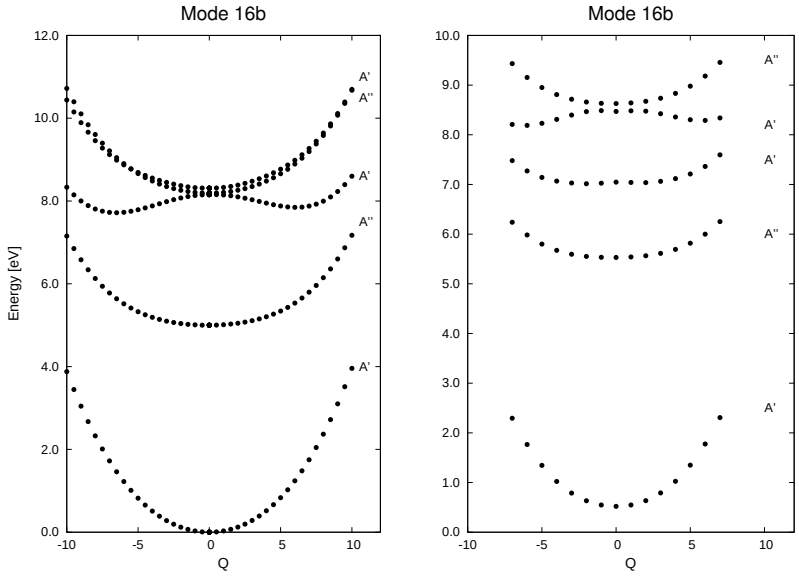

Fig. 6.5: Comparison of the the potential energy surface along mode $\upsilon 16_b$ between the CASSCF(6,6), left, calculations and the CASPT2(6,6),left, calculations. The energy of the 5th state (S_4) in the CASSCF calculations is significantly lower in the CASPT2 calculations making it the third state (S_2)

State	CASSCF(6,6)	CASPT2(6,6)	CASPT(6,7)	Experimental
s_1	5.00	5.01	4.74	4.65
s_2	8.16	6.52	5.87	
s_3	8.19	7.95	7.14	
s_4	8.31	8.11	7.25	

Table 6.2: A table comparing the energies of the first four excited states of toluene as calculated with CASSF(6,6), CASPT2(6,6) and CASPT2(6,7) methods and experimental values where available (in eV).

failing were those where significant ring deformations produced a considerable overlap with the in plane p orbitals on the methyl group (orbitals on the left in figure 6.6). The excited state energies calculated using the various methods and active spaces are shown in table 6.2.

The following modes were calculated using the 6,7 active space $\upsilon 10_b$,$\upsilon 6_b$,$\upsilon 18_a$,$\upsilon 9_a$,$\upsilon 19_a$ and $\upsilon 13$. As the state energies differed prior to and VCHAM fitting procedure all of the surfaces calculated using the CASPT2(6,6) active space were

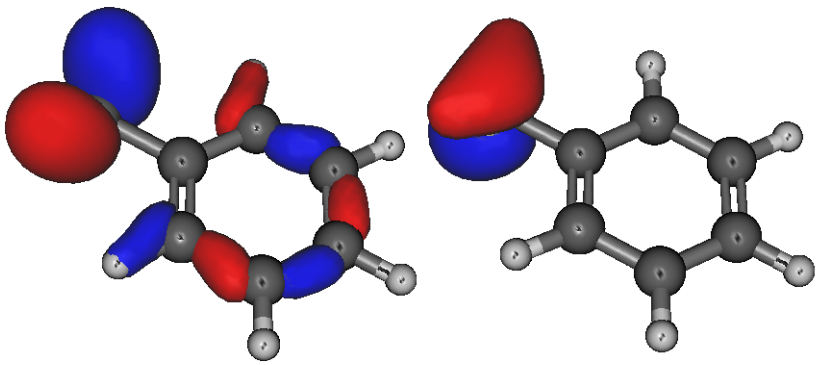

Fig. 6.6: Molecular orbitals based on the methyl group of toluene considered for inclusion in the active space. The molecular orbital on the left shows considerable in plane p character whereas the molecular orbital on the right shows out of plane p character.

shifted in energy to those calculated using the (6,7) active space.

6.3 Model Hamiltonian

Initial attempts to fit the VCHAM parameters to the calculated ab-intio reference points used only linear optimisation, but met with some difficulty. This is part led to the development of the Genetic Algorithm to fit these parameters. The Hamiltonian here was calulated using an initial genetic algorithm fitting procedure, running for 200 generations and an initial population of 1000, then a local optimiser was used to conclude the fitting. Example fits along three selected modes are shown in figure 6.7.

The following tables 6.3,6.4 and 6.5 show some of the coupling parameters arrived at by the fitting procedure.

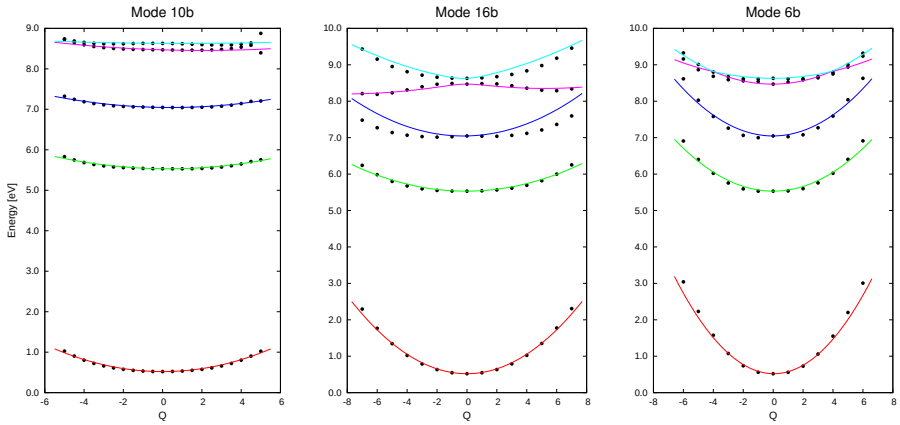

Fig. 6.7: Example cuts through the potential energy surface of toluene with the VCHAM fits overlaid. The cuts are along the vibrational modes $\upsilon 10_b$, $\upsilon 16_b$ and $\upsilon 6_a$ (left to right).

Mode	S_1
$\upsilon 10_b$	-
	0.00820
$\upsilon 16_b$	0.00793
$\upsilon 6_a$	0.00552
$\upsilon 6_b$	0.00710
$\upsilon 18_a$	-
	0.09160
$\upsilon 17_b$	-
	0.00056
$\upsilon 9_a$	0.12310
$\upsilon 12$	-
$\upsilon 13$	-
	0.07160

Table 6.3: A table showing the 1st order on-diagonal terms, κ of the VCHAM for some of the important vibrational modes of toluene

Mode	$S_1 - S_2$
$\upsilon 10b$	0.00100
$\upsilon 16b$	0.03840
$\upsilon 6a$	-
$\upsilon 6b$	-
$\upsilon 18a$	-
$\upsilon 17b$	-
$\upsilon 9a$	-
$\upsilon 12$	0.00070
$\upsilon 13$	-

Table 6.4: The 1st order off diagonal terms, λ, coupling with the first excited state of the VCHAM for some of the important vibrational modes of toluene

Mode	S_0	S_1
$\upsilon 10b$	0.01170	-0.00730
$\upsilon 16b$	0.03320	-0.04022
$\upsilon 6a$	0.08350	0.00035
$\upsilon 6b$	-0.00100	-0.01330
$\upsilon 18a$	-0.00330	-0.00910
$\upsilon 17b$	0.06670	-0.00637
$\upsilon 9a$	-0.00300	-0.00290
$\upsilon 12$	0.01790	0.00510
$\upsilon 13$	-0.00170	-0.00090

Table 6.5: The second order on diagonal, γ, terms of the VCHAM for some of the important vibrational modes of toluene

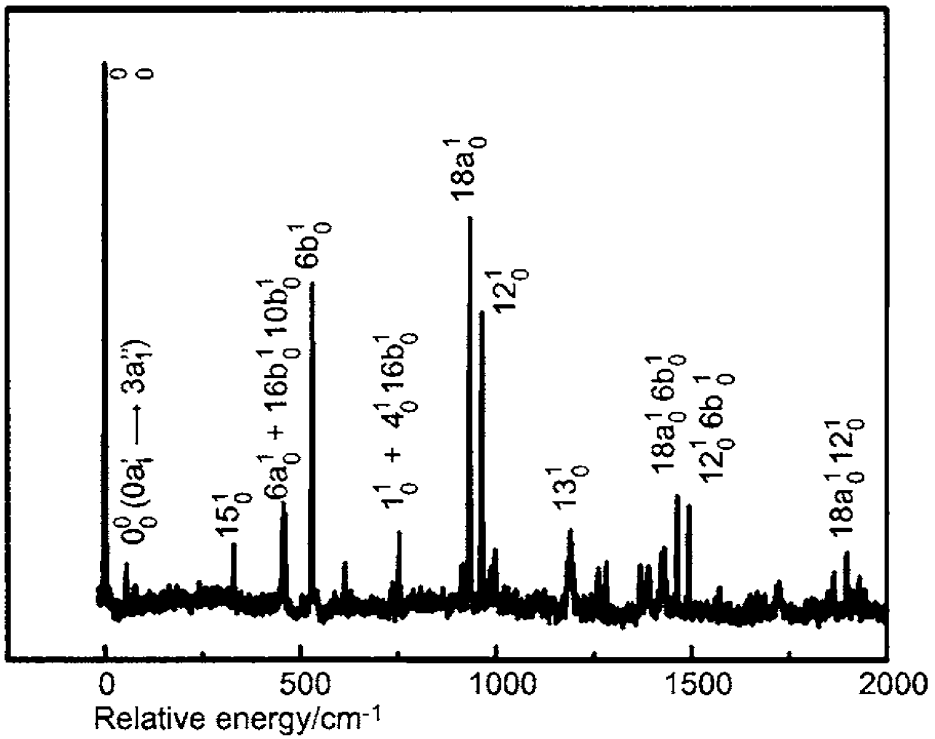

Fig. 6.8: Flourescence excitation spectrum of toluene in the region of the $S_1 - S_0(^1B_2 - ^1A_1)$ band reproduced from /citelawrance:1995.

6.4 Absorption Spectrum

In order to test the validity of the model it is useful to attempt to reproduce the experimental spectrum. For comparison the experimental spectrum reported by Lawrance [115] is shown in figure 6.8.

The following calculated spectra were all obtained by generating an initial wavepacket on the S_1 surface and allowing it to propagate. For each spectrum this propogation lasted for 500 fs and during the analysis a damping time of 500 fs was used and a damping factor of 1. The first spectrum, figure 6.9, uses only the first order and on-diagonal second order parameters (κ,λ and on diagonal γ).

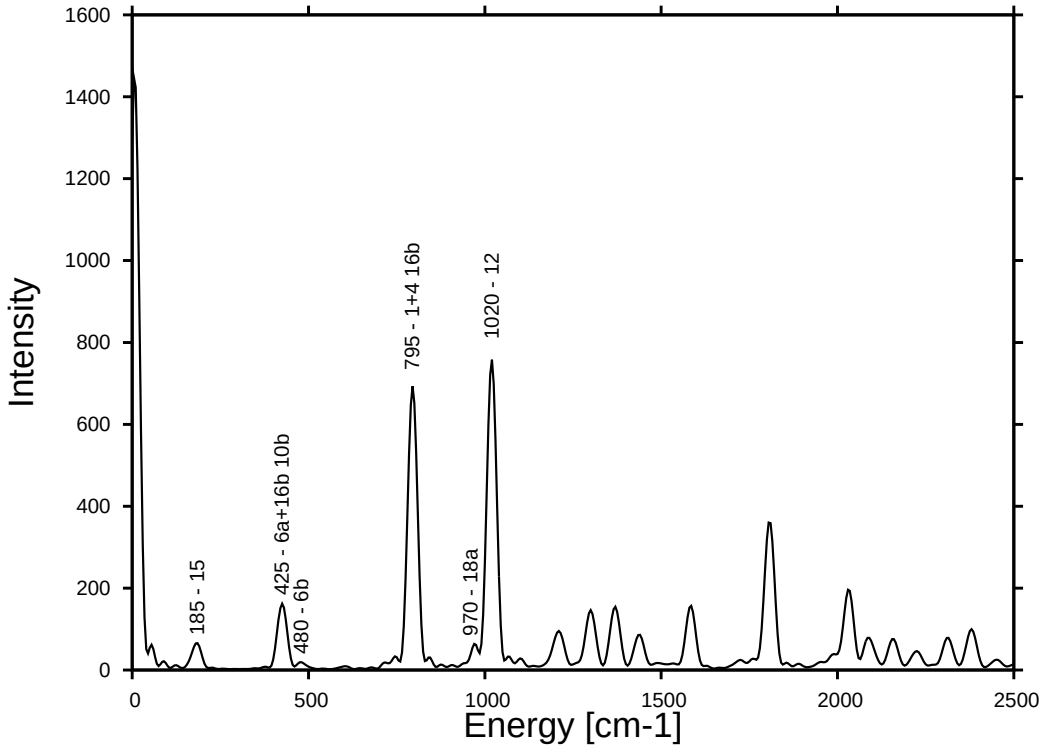

Fig. 6.9: A simulated absorption spectrum calculated using the toluene VCHAM with first order and on-diagonal second order parameters

By comparison with the experimental spectrum, in figure 6.8, we can see that many of the peaks have a very weak intensity. Most of these peaks are only visible in the absorption spectrum due to a large change in their transition dipole moment, or they are part of a double excitation peak where one of the relevent vibrations is only visible due to a large change in their transition dipole moment. These can be added by relaxing the initial wavepacket under the influence of a transition dipole moment operator fitted to calculations of the transition dipole moment along each vibration. This makes a significant difference to the absorption spectrum as shown in figure 6.10.

The transition dipole moment operator has visibly increased the intensity of 18a peak and more importantly has increased the intensity of the 6_a peak so it is no longer hidden underneath the 16_b10_b peak. This is important as these

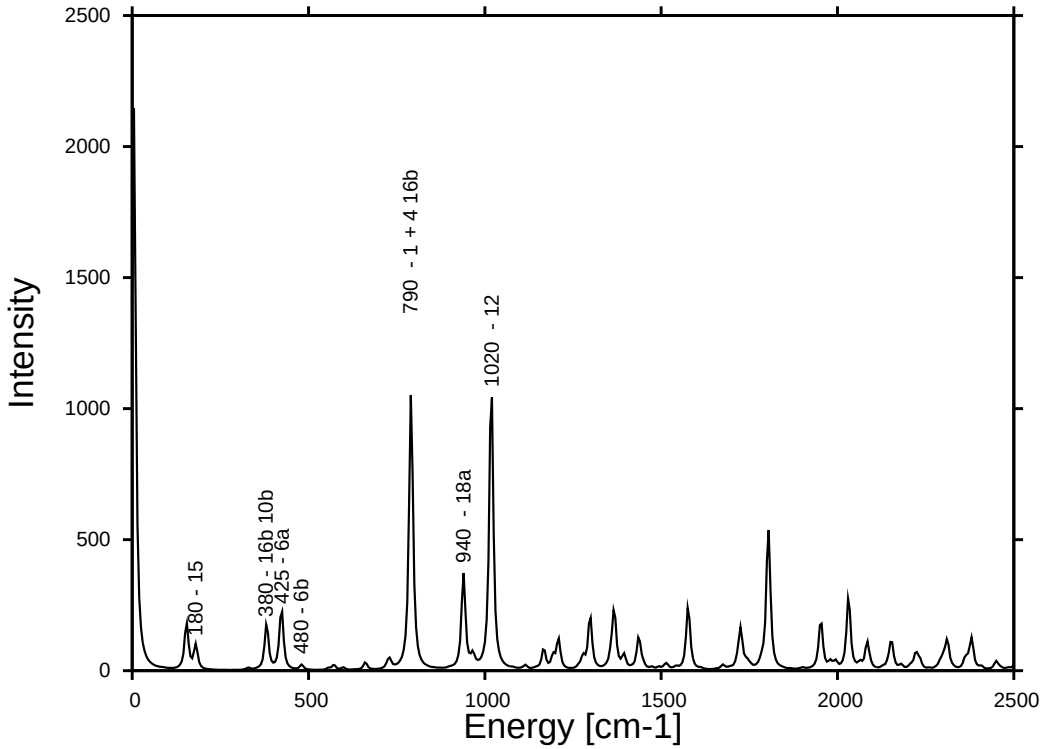

Fig. 6.10: A simulated absorption spectrum calculated using the toluene VCHAM with first order and on-diagonal second order parameters after using the transition dipole operator to relax the initial wavepacket

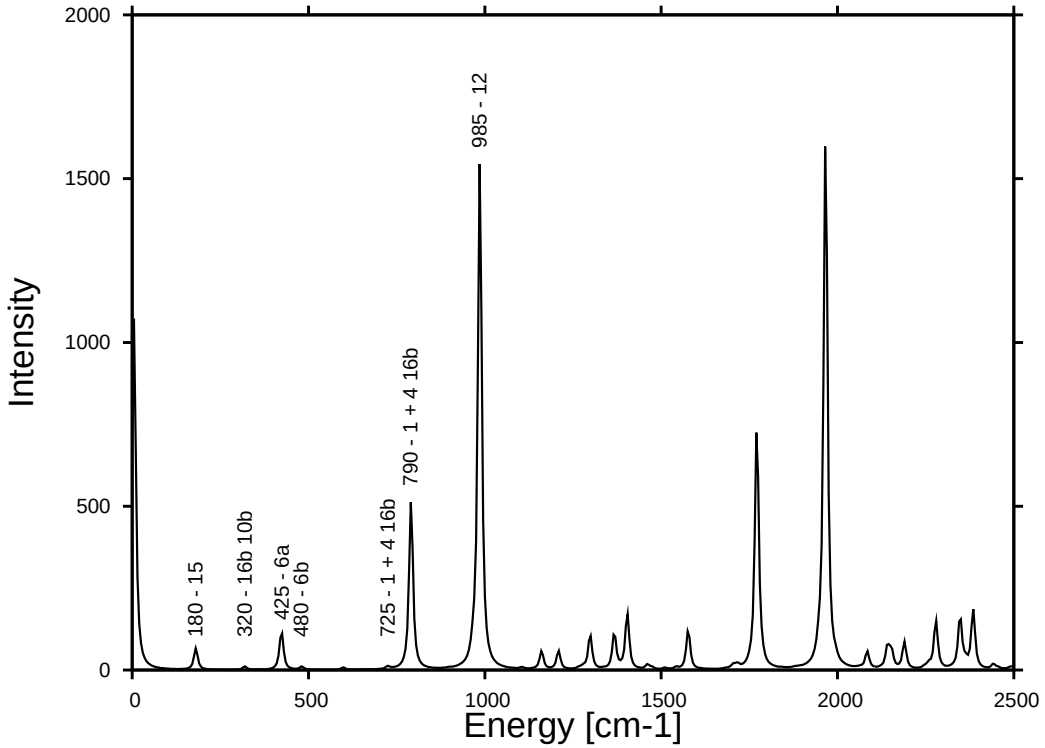

Fig. 6.11: A simulated absorption spectrum calculated using the off-diagonal second order toluene VCHAM after using the transition dipole operator to relax the initial wavepacket

three vibrations constitute the Fermi resonance detected experimentally. Although all of the important peaks are now visible their relative intensities still differ significantly from the experimental spectrum, figure 6.8. This can often be improved by improving the model to include higher order parameters. The spectrum in figure 6.11 shows the result of the inclusion of second-order off diagonal coupling terms.

6.5 Conclusion

Attempts to reproduce the absorption spectrum of toluene are qualitatively successful, all of the major peaks in the absorptions spectra are present. Their

relative intensities however remain a problem, one which was not solved by adding higher order terms. This is either due to the requirement for even higher order terms or of inaccurate representation of the diagonal cuts between vibrational modes. As the geometries were calculated away from the equilibrium geometry convergence failure became increasingly common.

Along vibrations where there were significant distortions, typically ring bending modes, a (6,7) active space was required. A larger active space may be required in order to calculate the geometries between vibrations in order to yield correct coupling terms for higher order parameters. Innacuracies in the PES, especially in a highly coupled system such as toluene, can lead to significant errors in the dynamic calculations.

Chapter 7

Conclusion

The three genetic algorithm test cases (cyclo-butadiene, allene and pentatetraene) were all fitted with relative ease. Both allene and pentatetraene were fitted to previous calculated PESs and were able to reproduce the experimental spectrum. This indicates that the sucess of the dynamic calculations presented here was the resut of an improved fit of the VCHAM. The sucess of the cyclo-butadiene test case in particular was important, as it shows the success of the genetic algorithm fitting method with a newly calculated PES. Although the Toluene surfaces were later optimised with the genetic algorithm additional time and effort was spent on the local optimisation stage than with the other test cases, making it unfair to compare it with cyclo-butadiene, allene and pentatetraene.

Calculating the excited states of toluene proved to be quite difficult and in-order to improve on the surfaces calculated in this thesis a significantly more computationally expensive method will most likely be required. The use of a reasonable basis set and a particularly high order method, namely CASPT2, suggests that improvment on teh calculation of these surfaces would require a significant invesment of computational resources aswell as a detailed study of the active orbitals required when moving away from the equilibrium ge-

ometry along certain modes.

The VCHAM was able to fit the calculated surfaces of toluene well which combined with the difficulties in the calculation of the PES suggests that innacuracies in the toluene dynamics calculations were liekly due to incorrect ab-initio potential energy surfaces. One problem with the VCHAM was that for a problem as large as toluene the number of parameters requiring optimisation became vast.

Bibliography

[1] Bryant, D. A. & Frigaard, N.-U. *Prokaryotic photosynthesis and phototrophy illuminated*. Trends in Microbiology, 2006. **14** (11), 488 – 496.

[2] Wayne, R. P. *Chemistry of Atmospheres: An Introduction to the Chemistry of the Atmospheres of Earth, the Planets, and Their Satellites*. Oxford University Press, Oxford, U.K., 2000.

[3] Atkins, P. W. *Atkins' Physical Chemistry*. Oxford University Press, Oxford, U.K., 2009.

[4] Atkins, P. W. *Molecular Quantum Mechanics 4nd edition*. Oxford University Press, Oxford, U.K., 2005.

[5] Zewail, A. H. *The birth of molecules (ultrafast photographic observations)*. Journal of Scientific America, 1990. **263** (6), 40–46.

[6] *Femptochemistry. Past, present, and future*.

[7] Dantus, M., Rosker, M. J., & Zewail, A. H. *Femtosecond real-time probing of reactions .2. The dissociation of ICN*, 1999. **89**, 6128.

[8] Meyer, H.-D., Gatti, F., & Worth, G. A., editors. *Multidimensional Quantum Dynamics: MCTDH Theory and Applications.*. Wiley, London, 2009.

[9] Jenson, F. *Introduction to Computational Chemistry*. John Wiley & Sons, Chichester, U.K., 1999.

[10] Markmann, A., Worth, G. A., & Cederbaum, L. S. *Allene and pentatetraene cations as models for intramolecular charge trans: Vibronic coupling Hamiltonian and conical intersections*. The Journal of Chemical Physics, 2005. **122**, 144,320.

[11] Markmann, A., Worth, G. A., & Mahapatra, S. *Simlation of a complex spectrum: Interplay of five electronic states and 21 vibrational degress of freedom*. The Journal of Chemical Physics, 2005. **123**, 204,310.

[12] Saddique, S. & Worth, G. *Applying the vibronic coupling model Hamiltonian to the photoelectron spectrum of cyclobutadiene*. J. Chem. Phys., 2006. **329**, 99–108.

[13] Kohn, D. & P.Chen. J. Am. Chem. Soc., 1993. **115**, 2844.

[14] Arnold, B. R. & Michl, J. *Ultraviolet and polarized infrared spectroscopy of matrix-isolated cyclobutadiene and its isotopomers*. The Journal of Physical Chemistry, 1993. **97** (50), 13,348–13,354.

[15] Meier, G. *Tetrahedrane and Cyclobutadiene*. Angew. Chem. Int. Ed., 1988. **27**, 309.

[16] Senn, P. *A simple quantum mechanical model that illustrates the Jahn-Teller effect*. Journal of Chemical Education, 1992. **69** (10), 819.

[17] Sancho-Garca, J., Prez-Jimnez, A., & Moscard, F. *A comparison between DFT and other ab initio schemes on the activation energy in the automerization of cyclobutadiene*. Chemical Physics Letters, 2000. **317** (35), 245 – 251.

[18] Nakamure, K., Osamura, Y., & Iwata, S. Chem. Phys., 1989. **136**, 67.

[19] Schrödinger, R. *An undulatory theory of the mechanics of atoms and molecules*. Physics Reviews, 1926. **28**, 1049–1070.

[20] Eckart, C. *The Kinetic Energy of Polyatomic Molecules*. Physics Reviews, 1934. **46**, 383–387.

[21] Tannor, D. J. *Introduction to Quantum Mechanics A Time Dependent Perspective*. University Science Books, Sausalito, California, USA, 2007.

[22] Born, M. & Fock, V. *Beweis des Adiabatensatzes*. Zeitschrift fr Physik A Hadrons and Nuclei, 1928. **51**, 165–180.

[23] Worth, G. A. & Cederbaum, L. *Beyond Born-Oppenheimer: Conical intersections and their impact on molecular dynamics.*.

[24] Levine, I. N. *Quantum Chemistry*. Pearson Prentice Hall, 2009.

[25] Harris, D. C. & Bertolucc, M. D. *Symmetry and Spectroscopy*. Oxford University Press, 1978.

[26] O'Brien, M. C. M. & Chancey, C. C. American Journal of Physics, 1993. **61**, 688–697.

[27] Yarkony, D. R. *Diabolical conical intersections*. Rev. Mod. Phys., Oct 1996. **68**, 985–1013.

[28] Bonnans, J., Gilbert, J., Lemarchal, C., & Sagastizbal, C. *Numerical optimization, theoretical and numerical aspects*. Springer, 2nd edition, 2006.

[29] Murty, K. G. *Linear programming*. John Wiley & Sons Inc., New York, 1983. ISBN 0-471-09725-X. With a foreword by George B. Dantzig.

[30] Avriel. *Nonlinear programming : analysis and methods*. Dover Publications, Mineola, NY, 2003. ISBN 0486432270.

[31] Land, A. H. & Doig, A. G. *An Automatic Method of Solving Discrete Programming Problems*. Econometrica, 1960. **28** (3), 497–520.

[32] Metropolis, N., Rosenbluth, A. W., Rosenbluth, M. N., Teller, A. H., & Teller, E. *Equation of State Calculations by Fast Computing Machines*. Journal of Chemical Physics, 1953. **21**, 1087–1092.

[33] Talbi. *Metaheuristics : from design to implementation*. John Wiley & Sons, Hoboken, N.J, 2009.

[34] Slater, N. B. *Theory of Unimolecular Reactions*. Ithaca, NY, 1959.

[35] Marcus, R. A. *Unimolecular Dissociations and Free Radical Recombination Reactions*. Journal of Physical Chemistry, 1952. **20**, 359.

[36] Dyson, F. J. *Statistical Theory of the Energy Levels of Complex Systems. I*. Journal of Mathematical Physics, 1962. **3**, 140.

[37] Bixon, M. & Jortner, J. *Intramolecular Radiationless Transitions*. Journal of Chemical Physics, 1968. **48**, 715.

[38] Kay, K. G. *Dynamical treatment of unimolecular decomposition reactions. The RRKM formula*. Journal of Chemical Physics, 1976. **64**.

[39] Hsiao, M. C., Sinha, A., & Crim, F. F. Journal of Chemical Physics, 1990. **92**, 6333.

[40] Themke, J. D., Sinha, A., & Crim, F. F. Journal of Chemical Physics, 1992. **96**, 372.

[41] Ratner, M. A. & Schatz, G. C. Prentice Hall, 2001.

[42] Cattarius, C., Worth, G., Meyer, H.-D., & Cederbaum, L. *All mode dynamics at the conical intersection of an octa-atomic molecule: Multi-configuration time-dependent Hartree (MCTDH) investigation on the butatriene cation*. Journal of Chemical Physics, 2001. **115**, 2088.

[43] Roothan, C. C. J. *New developments in molecular orbital theory*. Reviews in Modern Physics, 1951. pages 69–89.

[44] Slater, J. C. Physics Reviews, 1930. **36**, 57.

[45] Hehre, W. J., Stewart, R. F., & Pople, J. A. Journal of Chemical Physics, 1969. **51**, 2657–2665.

[46] Andersson, K., Malmqvist, P. A., Roos, B. O., Sadlej, A. J., & Wolinski, K. *Second-order perturbation theory with a CASSCF reference function*. The Journal of Physical Chemistry, 1990. **94** (14), 5483–5488.

[47] Roos, B. O. & Andersson, K. *Multiconfigurational perturbation-theory with level shift: The Cr_2 potential revisited*. Chemical Physics Letters, 1995. **245**, 215–223.

[48] *Phase transition for a hard sphere system*. B. Alder and T. Wainwright, 1957. **27**, 1208–1209.

[49] Alder, B. & Wainwright, T. *Studies in molecular dynamics 1 General Method*, 1959. **31**, 459–466.

[50] Rahman, A.

[51] Heller, E. J.

[52] Wyatt, R. E. & McCullough, E. A. *Quantum dynamics of the collinear (H,H_2) reaction*. Journal of Physical Chemistry, 1969. **51**, 1253.

[53] Kosloff, D. & Kosloff, R. *A Fourier-method solution for the time-dependent Schrödinger equation as a tool in molecular dynamics.*. Journal of Computational Physics, 1983. **52**, 35.

[54] Light, J. C. *Time-Dependent Quantum Molecular Dynamics*. Plenum, New York, USA.

[55] Harris, D. O., Engerholm, G. G., & Gwinn, G. W. *Calculation of matrix elements for one-dimensional quantum mechanical problems and the application to anharmonic oscillators*. Journal of Chemical Physics, 1965. **3**, 1515.

[56] Dickinson, A. S. & Certain, P. R. *Calculation of matrix elements for one-dimensional quantum mechanical problems*. Journal of Chemical Physics, 1968. **49**, 4209.

[57] Fletcher, R. *Practical Methods of Optimization*. Wiley, Chichester, U. K., 1981.

[58] Schlegel, H. B. *Optimization of Equilibrium Geometries and Transition Structures*. Journal of Computation Chemistry, 1983. **3**, 214–218.

[59] Li, X. & Frisch, M. J. *Energy represented DIIS with a hybrid geometry optimization method*. Journal of Chemical Theory and Computation, 2006. **2**, 835–839.

[60] *Systematic ab-initio gradient calculation of molecular geometries, force constants and dipole moment derivatives*. Journal of the American Chemical Society, 1979. **101**, 2550–2560.

[61] *Using redundant internal co-ordinates to optimize equilibrium geometries and transition states*. Journal of Computation Chemistry, 1996. **17**, 49–56.

[62] Frisch, M. J., Trucks, G. W., Schlegel, H. B., Scuseria, G. E., Robb, M. A., Cheeseman, J. R., Montgomery, J. A., Jr., Vreven, T., Kudin, K. N., Burant, J. C., Millam, J. M., Iyengar, S. S., Tomasi, J., Barone, V., Mennucci, B., Cossi, M., Scalmani, G., Rega, N., Petersson, G. A., Nakatsuji, H., Hada, M., Ehara, M., Toyota, K., Fukuda, R., Hasegawa, J., Ishida, M., Nakajima, T., Honda, Y., Kitao, O., Nakai, H., Klene, M., Li, X., Knox, J. E., Hratchian, H. P., Cross, J. B., Bakken, V., Adamo, C., Jaramillo, J., Gomperts, R., Stratmann, R. E., Yazyev, O., Austin, A. J., Cammi, R., Pomelli, C., Ochterski, J. W., Ayala, P. Y., Morokuma, K., Voth, G. A., Salvador, P., Dannenberg, J. J., Zakrzewski, V. G., Dapprich, S., Daniels, A. D., Strain, M. C., Farkas, O., Malick, D. K., Rabuck, A. D., Raghavachari, K., Foresman, J. B., Ortiz, J. V., Cui, Q., Baboul, A. G., Clifford, S., Cioslowski, J., Stefanov, B. B., Liu, G., Liashenko, A., Piskorz, P., Komaromi, I., Martin, R. L., Fox, D. J., Keith, T., Al-Laham, M. A., Peng, C. Y., Nanayakkara, A., Challacombe, M., Gill, P. M. W., Johnson, B., Chen, W., Wong, M. W., Gonzalez, C., & Pople, J. A. *Gaussian 03, Revision C.02*. Gaussian, Inc., Wallingford, CT, 2004.

[63] Simons, J. & Nichols, J. International Journal of Quantum Chemistry, 1990. **24**, 263.

[64] Pulay, P. Journal of Computational Chemistry, 1982. **3**, 556.

[65] et. al., M. *Allene and pentatetraene cations as models for intramolecular charge transfer: Vibronic coupling Hamiltonian and conical intersections*. Journal of Chemical Physics,, 2005.

[66] Hestenes, M. & Stiefel, E. *Methods of Conjugate Gradients for Solving Linear Systems*. J. Res. National Bureau of Standards, 1952. **49**, 409–436.

[67] Hartke, B. *Structural Transitions in Clusters*. Angew. Chem. Int. Ed., 2002. **41**, 1468–1487.

[68] Pittaway, F., Paz-Borbon, L., Johnston, R., Arslan, H., Ferrando, R., Mottet, C., Barcaro, G., & Fortunelli, A. *Theoretical Studies of Palladium-Gold Nanoclusters: Pd-Au Clusters with up to 50 Atoms*. J. Phys. Chem., 2009. **113**, 9141–9152.

[69] Rossi, G. & Ferrando, R. *Searching for low-energy structures of nanoparticles: a comparison of different methods and algorithms*. J. Phys.: Condens. Matter., 2009. **21**, 1–11.

[70] Falcioni, M. & Deem, M. *A biased Monte Carlo scheme for zeolite structure solution*. J. Phys. Chem., 1999. **110**, 1754–1766.

[71] P.Poulain, Calvo, F., Antoine, R., Broyer, M., & Dugourd, P. *Competition between secondary structures in gas phase polyalanines*. Europhys. Lett., 2007. **79**, 66,003.

[72] Iwamatsu, M. & Okabe, Y. *Basin Hopping with Occasional Jumping*. Chem. Phys. Lett., 2008. **399**, 396–400.

[73] Wales, D. & Doye, J. *Global Optimization by Basin-Hopping and the Lowest Energy Structures of Lennard-Jones Clusters Containing up to 110 Atoms*. J. Phys. Chem., 1997. **101**, 5111–5116.

[74] Nayeem, Vila, & Scherga. J. Comp. Chem., 1991. **12**, 594–605.

[75] Kirkpatrick, Gelatt, & Vecchi. Science, 1983. **220**, 671–680.

[76] Wenzel & Hamacher. *Stochastic tunneling approach for global optimization of complex potential energy surfaces*. Phys. Rev. Lett., 1999. **82**, 3003.

[77] Hu, X.-M., Zhang, Z., & Li, Y. *Orthogonal Methods Based Ant Colony Search for Solving Continuous Optimization Problems*. J. Comp. Sci. Tech., 2008. **23**, 2–18.

[78] Call, S., Zubarev, D., & Boldyrev, A. *Global Minimum Structure Searches via Particle Swarm Optimization*. J. Comp. Chem., 2006. **28**, 1177–1186.

[79] Pham, D., Ghanbarzadeh, A., Otri, S., & Koç, E. *Optimal design of mechanical components using the Bees Algorithm*. J. Mech. Eng. Sci., 2009. **223**, 1051–1056.

[80] Kekulé, A. Liebigs Ann. Chem., 1872. **162**, 77.

[81] Metropolis, A. & Chiu, Y.-N. J. Mol. Struct. (Theochem), 1996. **365**, 119.

[82] Roeselov/'a, M., Bally, T., Jungwirth, P., & Čárksy, P.

[83] Bally, T. & Masamune, S. *Cyclobutadiene*. Tetrahedron, 1979. **26**, 343–378.

[84] Maier, G. Angew. Chem. Int. Ed., 1974. **13**, 425.

[85] Maier, G., Hartan, H.-G., & Sayrac, T. Angew. Chem. Int. Ed., 1976. **15**, 226.

[86] Whittle, E., Dows, D., & Pimentel, G. J. Chem. Phys., 1954. **22**, 1943.

[87] Norman, I. & Porter, G. Nature, London, 1954. **174**, 508.

[88] Allinger, N., Gilardeau, C., & Chow, L. Tetrahedron, 1968. **24**, 2401.

[89] Allinger, N. & Tai, J. Theor. Chem. Acta, 1968. **12**, 29.

[90] Frisch, M. J., Trucks, G. W., Schlegel, H. B., Scuseria, G. E., Robb, M. A., Cheeseman, J. R., Scalmani, G., Barone, V., Mennucci, B., Petersson, G. A., Nakatsuji, H., Caricato, M., Li, X., Hratchian, H. P., Izmaylov, A. F., Bloino, J., Zheng, G., Sonnenberg, J. L., Hada, M., Ehara, M., Toyota, K., Fukuda, R., Hasegawa, J., Ishida, M., Nakajima, T., Honda, Y., Kitao, O., Nakai, H., Vreven, T., Montgomery, J. A., Jr., Peralta, J. E., Ogliaro, F., Bearpark, M., Heyd, J. J., Brothers, E., Kudin, K. N., Staroverov, V. N., Kobayashi, R., Normand, J., Raghavachari, K., Rendell, A., Burant, J. C., Iyengar, S. S., Tomasi, J., Cossi, M., Rega, N., Millam, J. M., Klene, M., Knox, J. E., Cross, J. B., Bakken, V., Adamo, C., Jaramillo, J., Gomperts, R., Stratmann, R. E., Yazyev, O., Austin, A. J., Cammi, R., Pomelli, C., Ochterski, J. W., Martin, R. L., Morokuma, K., Zakrzewski, V. G., Voth, G. A., Salvador, P., Dannenberg, J. J., Dapprich, S., Daniels, A. D., Farkas, ., Foresman, J. B., Ortiz, J. V., Cioslowski, J., & Fox, D. J. *Gaussian 09 Revision A.1*. Gaussian Inc. Wallingford CT 2009.

[91] Werner, H.-J., Knowles, P. J., Manby, F. R., Schütz, M., Celani, P., Knizia, G., Korona, T., Lindh, R., Mitrushenkov, A., Rauhut, G.,

Adler, T. B., Amos, R. D., Bernhardsson, A., Berning, A., Cooper, D. L., Deegan, M. J. O., Dobbyn, A. J., Eckert, F., Goll, E., Hampel, C., Hesselmann, A., Hetzer, G., Hrenar, T., Jansen, G., Köppl, C., Liu, Y., Lloyd, A. W., Mata, R. A., May, A. J., McNicholas, S. J., Meyer, W., Mura, M. E., Nicklass, A., Palmieri, P., Pflüger, K., Pitzer, R., Reiher, M., Shiozaki, T., Stoll, H., Stone, A. J., Tarroni, R., Thorsteinsson, T., Wang, M., & Wolf, A. *MOLPRO, version 2010.1, a package of ab initio programs*, 2010. See http://www.molpro.net.

[92] Cederbaum, L. S. Journal of Physics B, 1975. **8**, 290.

[93] von Niessen, W., Schirmer, J., & Cederbaum, L. S.

[94] Frisch, M. J., Trucks, G. W., Schlegel, H. B., Scuseria, G. E., Robb, M. A., Cheeseman, J. R., Zakrzewski, V. G., Jr., J. A. M., Stratmann, R. E., Burant, J. C., Dapprich, S., Millam, J. M., Daniels, A. D., Kudin, K. N., Strain, M. C., Farkas, O., Tomasi, J., Barone, V., Cossi, M., Cammi, R., Mennucci, B., Pomelli, C., Adamo, C., Clifford, S., Ochterski, J., Petersson, G. A., Ayala, P. Y., Cui, Q., Morokuma, K., Salvador, P., Dannenberg, J. J., Malick, D. K., Rabuck, A. D., Raghavachari, K., Foresman, J. B., Cioslowski, J., Ortiz, J. V., Baboul, A. G., Stefanov, B. B., Liu, G., Liashenko, A., Piskorz, P., Komaromi, I., Gomperts, R., Martin, R. L., Fox, D. J., Keith, T., Al-Laham, M. A., Peng, C. Y., Nanayakkara, A., Challacombe, M., Gill, P. M. W., Johnson, B., Chen, W., Wong, M. W., Andres, J. L., Gonzalez, C., Head-Gordon, M., Replogle, E. S., & Pople, J. A. *Gaussian 98*. Gaussian, Inc., Pittsburgh, PA, 1998.

[95] Schirmer, J., Cederbaum, L. S., & Walter, O. Physics Reviews A. **28**, 1237.

[96] Baltzer, P., Wannberg, B., Lundquist, M., Holland, L. K. D. M. P., MacDonald, M. A., & von Niesson, W. Chemical Physics, 1995. **196**, 551.

[97] Bieri, G., Dill, J. D., Heilbronner, E., Maier, J. P., & Ripoll, J. L. Helvetica Chimica Acta, 1977. **60**, 629.

[98] Bryce-Smith, D. & Gilbert, A. *The organic photochemistry of benzeneI*. Tetrahedron, 1976. **32** (12), 1309 – 1326.

[99] Philis, J., Bolovinos, A., Andritsopoulos, G., Pantos, E., & Tsekeris, P. *A comparison of the absorption spectra of the fluorobenzenes and benzene in the region 4.5 - 9.5 (eV)*. Journal of Physics B, 1981. **14**, 3621–3635.

[100] Parmenter, C. S. *Radiative and Nonradiative Processes in Benzene*. Advances in Chemical Physics, 1972. **22**, 365–421.

[101] Clara, M., Hellerer, T., & Neusser, H. J. *Fast decay of high vibronic S_1 states in gas-phase benzene*. Applied Physics B, 2000. **71**, 431.

[102] Toniolo, A., Thompson, A. L., & Marťinez, T. *Excited state direct dynamics of Benzene with parametrized multi-reference semiempirical configuration interaction methods*. Chem. Phys., 2004. **304**, 133–145.

[103] Roos, B. O., Andersson, K., & Fülscher, M. P. *Towards and accurate molecular orbital theory for excited states: the benzene molecule*. Chem. Phys. Lett., 1992. **192**, 5–13.

[104] G.A. & Worth. *A model Hamiltonian to simulate the complex photochemistry of benzene*. Journal of Photochemistry and Photobiology A: Chemistry, 2007. **190** (2-3), 190 – 199.

[105] Penfold, T. J. & Worth, G. A. *A model Hamiltonian to simulate the complex photochemistry of benzene II*. Journal of Chemical Physics, 2009. **131**, 064,303.

[106] Ginsburg, N., Robertson, W. W., & Matsen, F. A. *The Near Ultraviolet Absorption Spectrum of Toluene Vapour*. Journal of Chemical Physics, 1946. **14**.

[107] Holtzclaw, K. W. & Parmenter, C. S. Journal of Chemical Physics, 1985. **83**, 1099.

[108] Jr., D. L. C., Holtzclaw, K. W., Krajnovich, D., Moss, D. B., Lawrance, W. D., Parmenter, C. S., & Knight, A. E. W. Journal of Physical Chemistry, 1985. **89**, 1577.

[109] Holtzclaw, K. W. & Parmenter, C. S. Journal of Chemical Physics, 1985. **82**, 5284.

[110] Parmenter, C. S. & Stone, B. M. *The methyl rotor as an accelerating functional group of IVR*. Journal of Chemical Physics, 1986. **84**.

[111] The Journal of Chemical Physics, 2005. **123**.

[112] The Journal of Chemical Physics, 2005. **123**.

[113] Hammond, C. J., Reid, K. L., & Ronayne, K. L. *Observation of a simple vibrational wavepacket ina polyatomic molecule via time-resolved photoelectron velocity-map imaging: A prototype for time-resolved IVR studies*. The Journal of Chemical Physics, 2006. **124**, 201,102.

[114] *Deducing anharmoinc coupling matrix elements from picosecond time-resolved photoelectron spectra: application to S_1 toluene at low vibra-*

tional energy. Physical Chemistry Chemical Physics, 2010. **12**, 9872–9883.

[115] Christopher G. Hickman, J. R. G. & Lawrance, W. D. *The $S_1S_0(^1B_2{}^1A_1)$ transition of jetcooled toluene: Excitation and dispersed fluorescence spectra, fluorescence lifetimes, and intramolecular vibrational energy redistribution*. Journal of Chemical Physics, 1996. **104**, 4887.